Coseismic fault-related fold model, growth structure, and the historic multisegment blind thrust earthquake on the basement-involved Yoro thrust, central Japan

Tatsuya Ishiyama,[1] Karl Mueller,[2] Hiroshi Sato,[3] and Masami Togo[4]

Received 6 March 2006; revised 16 January 2007; accepted 5 February 2007; published 28 March 2007.

[1] We use high-resolution seismic reflection profiles, boring transects, and mapping of fold scarps that deform late Quaternary and Holocene sediments to define the kinematic evolution, subsurface geometry, coseismic behavior, and fault slip rates for an active, basement-involved blind thrust system in central Japan. Coseismic fold scarps on the Yoro basement-involved fold are defined by narrow fold limbs and angular hinges on seismic profiles, suggesting that at least 3.9 km of fault slip is consumed by wedge thrust folding in the upper 10 km of the crust. The close coincidence and kinematic link between folded horizons and the underlying thrust geometry indicate that the Yoro basement-involved fold has accommodated slip at an average rate of 3.2 ± 0.1 mm/yr on a shallowly west dipping thrust fault since early Pleistocene time. Past large-magnitude earthquakes, including an historic M∼7.7 event in A.D. 1586 that occurred on the Yoro blind thrust, are shown to have produced discrete folding by curved hinge kink band migration above the eastward propagating tip of the wedge thrust. Coseismic fold scarps formed during the A.D. 1586 earthquake can be traced along the en echelon active folds that extend for at least 60 km, in spite of different styles of folding along the apparently hard-linked Nobi-Ise blind thrust system. We thus emphasize the importance of this multisegment earthquake rupture across these structures and the potential risk for similar future events in en echelon active fold and thrust belts.

Citation: Ishiyama, T., K. Mueller, H. Sato, and M. Togo (2007), Coseismic fault-related fold model, growth structure, and the historic multisegment blind thrust earthquake on the basement-involved Yoro thrust, central Japan, *J. Geophys. Res.*, *112*, B03S07, doi:10.1029/2006JB004377.

1. Introduction

[2] Long-term and coseismic growth of active folds can be used as a proxy for slip produced during earthquakes on blind thrusts. Studies of many active fold and thrust belts such as those in Taiwan and the Himalaya show that deformation of fluvial terraces within transverse channels can also be used to define styles and rates of active folding, in effect providing finite strain markers of different age across these structures [*Philip and Meghraoui*, 1983; *Rockwell et al.*, 1984, 1988; *Bullard and Lettis*, 1993; *Molnar et al.*, 1994; *Burbank et al.*, 1996; *Shaw and Suppe*, 1996; *Mueller and Suppe*, 1997; *Benedetti et al.*, 2000, 2003; *Lavé and Avouac*, 2000; *Thompson et al.*, 2002; *Dolan et al.*, 2003; *Ishiyama et al.*, 2004; *Bennett et al.*, 2005; *Shyu et al.*, 2006; *Scharer et al.*, 2006]. In particular, studies by *Lavé and Avouac* [2000], *Ishiyama et al.* [2004] and other papers in this special section show that folded fluvial terraces can be related to overall fold geometry and the kinematics of migrating axial surfaces or wholesale rotation of fold limbs. This can then be used to identify the mechanisms that act to build fault-related folds, determine the geometry of blind thrusts and track the accrual of slip on them. This approach points to the significance of tectonic landforms and their utility in recording growth of active folds at different timescales, providing a geomorphic record of slip on underlying blind thrusts. Moreover, because blind thrusts do not reach the ground surface, the kinematic linkage between fold scarps and underlying thrusts is implicit and hence must be carefully documented in order to validate estimates of fault slip as provided by inversions of seismological or geodetic data [cf. *Freymueller et al.*, 1994; *Johnson et al.*, 2001; *Dominguez et al.*, 2003]. This is also of obvious importance for assessing the styles of surface deformation produced along active folds for seismic hazards analysis in urbanized areas [*Mueller et al.*, 1999; *Suppe et al.*, 2000; *Champion et al.*, 2001; *Hung and Suppe*, 2002; *Dolan et al.*, 2003; *Ishiyama et al.*, 2004].

[3] Kinematic models of fault-related folds, which are broadly assigned to those that grow by fault bend [*Suppe*, 1983; *Medwedeff*, 1992; *Medwedeff and Suppe*, 1997] and

[1]Active Fault Research Center, Geological Survey of Japan, National Institute of Advanced Industrial Science and Technology, Tsukuba, Japan.
[2]Department of Geological Sciences, University of Colorado, Boulder, Colorado, USA.
[3]Earthquake Research Institute, University of Tokyo, Tokyo, Japan.
[4]Department of Geoscience, Hosei University, Machida, Japan.

0148-0227/07/2006JB004377$09.00

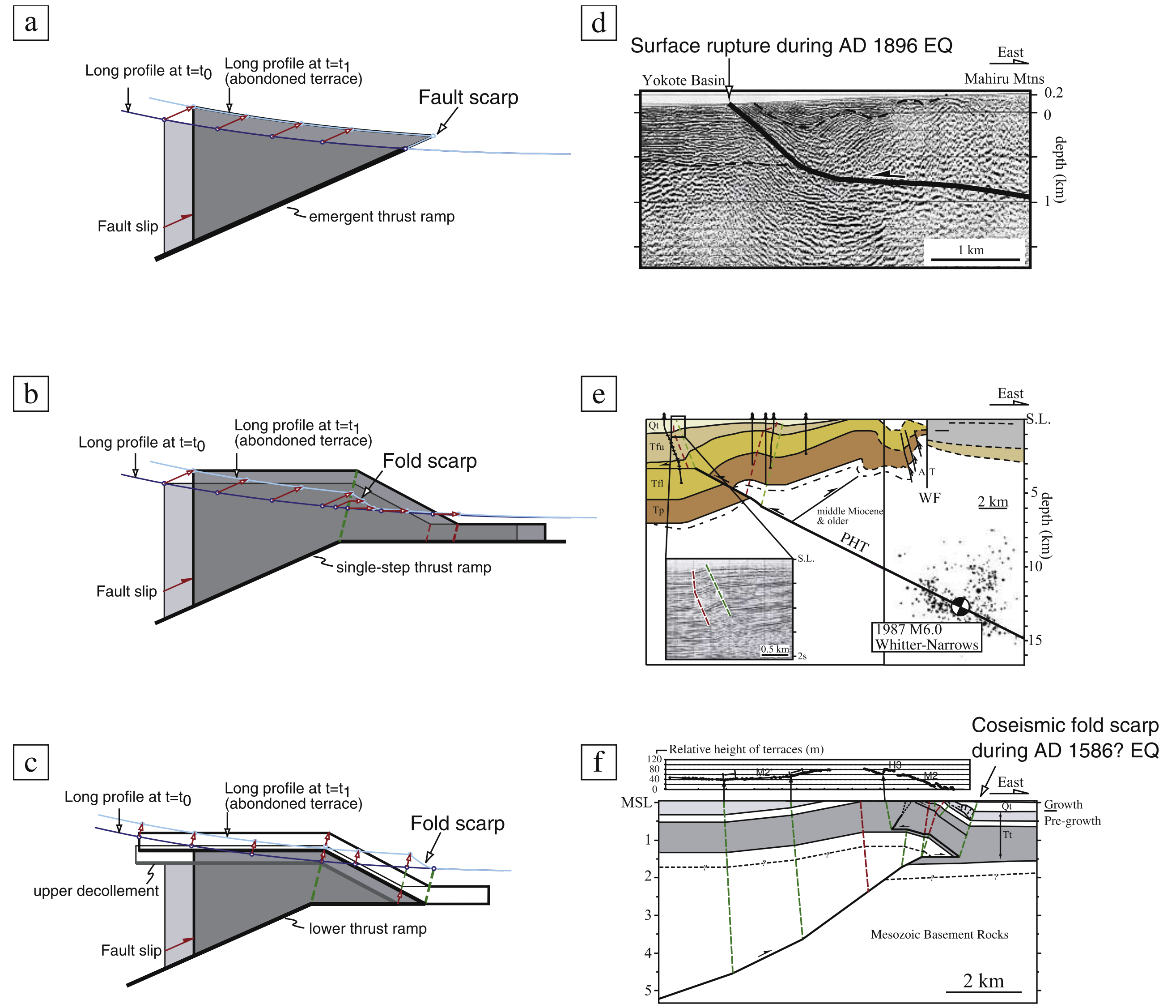

Figure 1. Schematic cross sections showing kinematic link between coseismic fold/fault scarps and geometries of underling thrusts in case of (a) emergent thrust ramp, (b) single-step fault bend fold [*Suppe*, 1983], and (c) wedge thrust fold [*Medwedeff*, 1992]. (d) Seismic reflection profile across a coseismic fault scarp during A.D. 1896 Riku-u earthquake (M 7) above an emergent thrust ramp [*Sato et al.*, 1997]. (e) Cross section across the Puente Hills thrust shows coseismic fold scarp above a ramp flat thrust trajectory [*Shaw et al.*, 2002; *Dolan et al.*, 2003]. (f) Cross section across Kuwana anticline in central Japan shows A.D. 1586 coseismic fold scarp above a doubly vergent thrust wedge [*Ishiyama et al.*, 2004]. Open-headed arrows indicate folding vectors.

trishear fault propagation mechanisms [*Erslev*, 1991; *Hardy and Ford*, 1997; *Allmendinger*, 1998], generally predict several different styles of surface strain related to overall fold and blind thrust geometry. Stratigraphic growth architecture [*Suppe et al.*, 1992; *Shaw and Suppe*, 1994; *Suppe et al.*, 1997] has also provided considerable insight into fold kinematics and their growth histories. A common style of coseismic fault-related folding includes growth of a fold scarp by shear above a blind thrust fault tip that propagates upward with increased displacement. Fold scarps formed as forelimbs of fault propagation folds [*Erslev*, 1991; *Allmendinger*, 1998] are documented for a number of thrust faults that have ruptured in large historic or prehistoric earthquakes (Figures 1a and 1d) [*Sato et al.*, 1997; *Champion et al.*, 2001; *Dolan et al.*, 2003; *Lee et al.*, 2004]. Other styles of coseismic folding can be distinguished by the location of active folding of the ground surface relative to the geometry of the fold limb. Fold scarps that grow at their crests by kink band migration are often related to folding across the top of a blind thrust ramp [*Suppe*, 1983; *Pratt et al.*, 2002; *Shaw et al.*, 2002; *Dolan et al.*, 2003] (Figures 1b and 1e). Alternatively, fold scarps that grow by surface folding across a synclinal axial surface, which we describe here for the Yoro fault, can often be related to wedge thrust faulting, where sediment and landforms is drawn upward onto the forelimb [*Medwedeff*, 1992; *Mueller and Suppe*, 1997; *Ishiyama et al.*, 2004] (Figures 1c and 1f). Secondary strain is also a common aspect of coseismic fault-related folding and

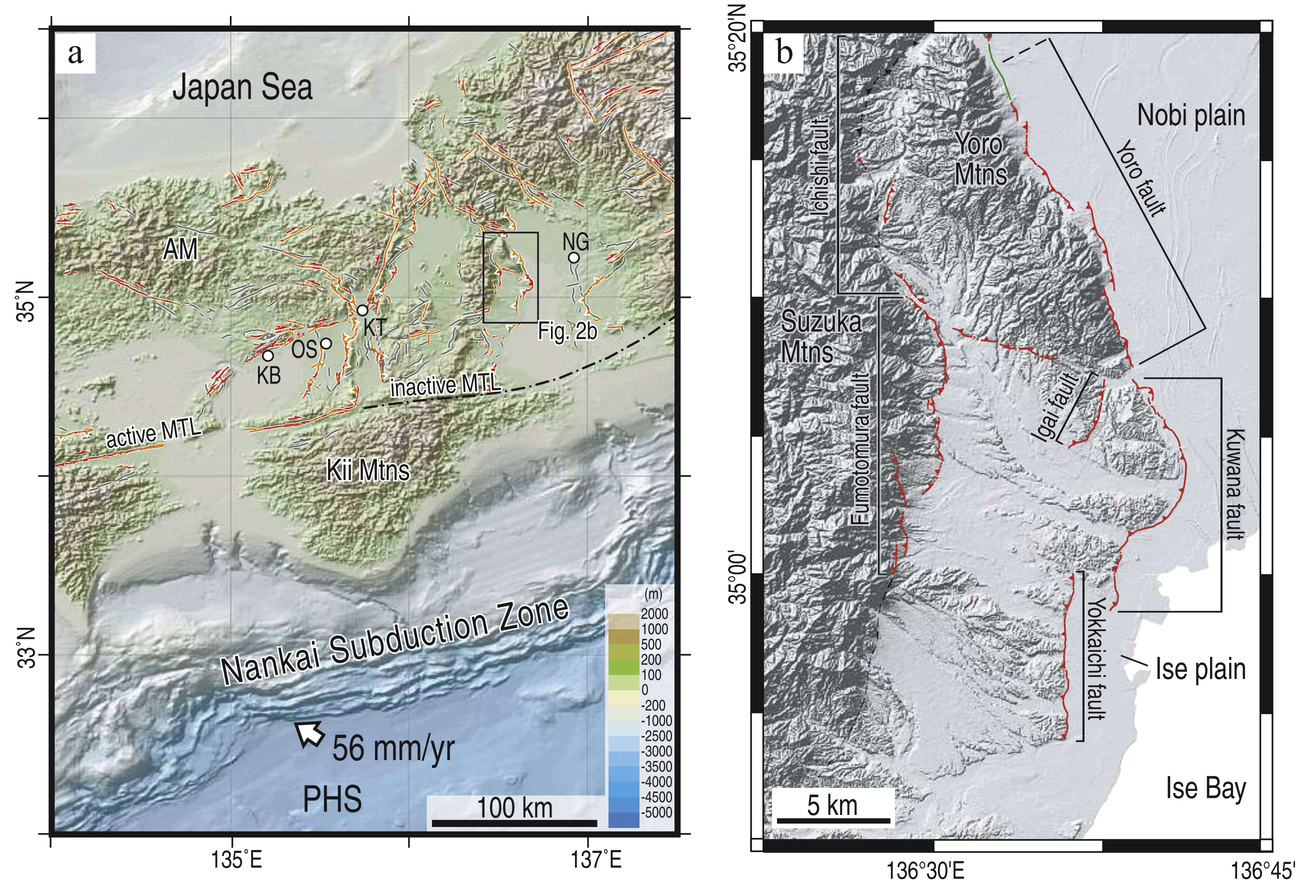

Figure 2. (a) Shaded relief map based on 250 m digital elevation model (DEM) [*Kishimoto*, 2000] showing the topography and distribution of active faults within the Kinki region, central Japan. Locations of active faults are from *Nakata and Imaizumi* [2002]. Red, orange, and gray lines mark active faults that are precisely located, approximately located, and inferred, respectively. Barbs denote hanging walls of active thrusts. Arrows indicate slip directions of strike-slip faults. Plate convergence rate is from *Wei and Seno* [1998]. Abbreviations for metropolitan areas are KB, Kobe; OK, Osaka; KT, Kyoto; NG, Nagoya. (b) Shaded relief map based on a 6-m DEM showing the locations of active thrusts in the northern portion of the NIFZ. Barbs indicate hanging walls of active thrusts.

includes small-scale extensional faulting [*Kelson et al.*, 1996; *Champion et al.*, 2001; *Philip et al.*, 1992] and flexural slip faulting [*Philip and Meghraoui*, 1983; *Ishiyama et al.*, 2004]. These features result from strain accumulation within forelimbs associated with coseismic slip but are not otherwise directly linked with slip on underlying blind thrusts or active axial surfaces extending from them.

[4] We argue therefore that careful description of coseismic fold scarps, coupled with data sets that define larger fold structure at different scales provides unambiguous structural solutions. Using this method, *Ishiyama et al.* [2004] showed that Kuwana anticline in the Nobi-Ise fault zone (NIFZ) in central Japan has formed as a wedge thrust fold and accommodated shortening during a historic blind thrust earthquake in A.D. 1586, which is expressed as a narrow kink band in late Holocene sediments.

[5] In this paper, we present additional data and new structural models of coseismic folding and fault-related fold of the Yoro basement-involved structure within the NIFZ in central Japan (Figure 2). Here we focus on coseismic fold scarps along an active fold and thrust belt that deform well-dated late Quaternary deposits, recording strain rates at different timescales and paleoearthquakes. Subsurface fold geometry is first constrained by high-resolution seismic profiles that image shallow (to depth of ~2.5 km) and very shallow (to depth of ~50 m) Pliocene, Pleistocene, and Holocene deposits. Secondly, detailed stratigraphy and age constraints of strata defined in boreholes drilled across late Holocene fold scarps reveal the near-surface (to depth of ~10 m) geometry of folded strata and timing of coseismic fold growth events that are correlated with earthquakes recorded in historic documents [*Usami*, 2003] and older paleoearthquakes. Third, two seismic reflection profiles across the forelimb and backlimb of the fold illuminate subsurface thrust trajectories beneath the basement-involved fold. This multiscale data set provides relatively unambiguous comparison between coseismic fold scarps generated by historically documented earthquakes with underlying fault-related fold geometry. Our work thus adds to the growing number of studies that test assumptions for fold kinematics by documentation of active structures known to grow in large blind thrust earthquakes [*Suppe et al.*, 2000;

Hung and Suppe, 2002; *Dolan et al.*, 2003; *Ishiyama et al.*, 2004]. The Yoro structure is particularly interesting because of the behavior during the A.D. 1586 earthquake, which apparently ruptured across at least two, and probably three separate fault-related folds in an en echelon pattern at the surface.

2. Regional Setting of the Yoro Basement-Involved Fold

[6] The Island of Honshu in central Japan is an actively deforming island arc with a complex array of strike slip and thrust faults that accommodate intraplate strain above subducting slabs of oceanic lithosphere. These fault systems often bound, or lie within Neogene sedimentary basins that are densely urbanized [*Research Group for Active Faults*, 1991; *Okada and Togo*, 2000; *Ikeda et al.*, 2002; *Nakata and Imaizumi*, 2002] (Figure 2). The Kinki region, located at central southwestern Honshu Island, is also characterized by an array of north trending thrust sheets, which have deformed Neogene basin deposits [*Yeats et al.*, 1997; *Ikeda et al.*, 2002; *Ishiyama et al.*, 2004]. The Kinki region lies between a Mesozoic accretionary wedge in central southwestern Japan and high-grade metamorphic rocks bounded by the Median Tectonic Line (MTL), a major dextral fault system to the south. E-W contraction north of the MTL in this region has occurred during late Cenozoic time where strain is partitioned above the obliquely subducting Philippine Sea plate (Figure 2a).

[7] The NIFZ consists of a 110-km-long array of active east verging thrusts that deform Neogene basins at the eastern edge of the Kinki region. The northern half of this thrust system includes (from north to south) the Yoro basement-involved fold, Kuwana anticline [*Ishiyama et al.*, 2004] and Yokkaichi anticline to the south (Figure 2b and 3). Shortening in this region also occurs along the Fumotomura and Ichishi faults, which contain the Suzuka Mountains in their hanging walls. Structural and surface relief of folds in the frontal NIFZ decreases from north to south.

[8] The Yoro basement-involved fold extends for 20 km in the northern NIFZ and separates the modern Nobi basin in the east from a piggyback portion of the basin and the Suzuka Mountains in the west (Figures 2b and 3). The Yoro Mountains form the stripped core of the largest structure in the NIFZ and expose Triassic-Jurassic strata that are translated eastward on a blind thrust above a 1500-m-thick sequence of Pliocene-Pleistocene strata deposited in the Nobi basin (Figures 4, 5, 6, and 7). The blind thrust underlying the Yoro Mountains is a part of a larger system of east vergent faults that includes the Ichishi thrust to the east. The Ichishi fault is the northern portion of the 20-km-long Fumotomura fault [*Ishiyama et al.*, 1999] that extends along the length of the northern NIFZ.

[9] The Suzuka Mountains, which lie in the hanging wall of the Fumotomura fault, have been thrust over a 1000-m-thick sequence of older, Pliocene–lower Pleistocene strata in the paleo-Nobi basin (Figures 8 and 9). In contrast to the Fumotomura and Yoro fault, the Ichishi thrust generally has not recently formed fold scarps along it, suggesting that it has been essentially inactive in late Pleistocene time. Thus the Yoro and Ichishi thrust faults can be interpreted as a forward breaking imbricate thrust system, although this is not the case further south where the Fumotomura fault appears to be presently active in addition to the frontal Kuwana and Yokkaichi anticlines.

3. Stratigraphy of the Nobi Basin and Its Piggyback Remnant

[10] As described in detail by *Ishiyama et al.* [2004], the Nobi basin is underlain by a >1500-m-thick succession of Pliocene to Holocene sediments. We used stratigraphy characterized in 600- and 1500-m-deep, continuously cored boreholes (GS-NB1 and Kz) in the Nobi basin (*Sugai et al.*'s [1999b] Figure 4; see their locations in Figure 3) to define the ages of reflectors in several seismic profiles. Pregrowth strata of Neogene age include fluvial and lacustrine sediments of the late Pliocene–early Pleistocene Tokai Group [*Takemura*, 1985; *Yoshida et al.*, 1991]. The Tokai Group in the Nobi basin is about 1500- to 2000-m-thick [*Committee for Subsurface Structure of the Nobi Plain*, 2001]. Dating of volcanic ash layers by the fission track method indicates that the Tokai Group was deposited from circa 2.8 Ma to 1.0 Ma [*Takemura*, 1985; *Yoshida et al.*, 1991] (Figure 4).

[11] Seismic reflection data presented later in this paper (Figure 5, 6, 7, and 9) suggest that reflectors correlated with late Pliocene–early Pleistocene sandstone and mudstone beneath the Nobi basin were deposited prior to uplift of the fold. Evidence for the pregrowth nature of these strata includes the continuity of units with a consistent thickness in the footwall syncline below, and in a piggyback basin uplifted onto the backlimb of the Yoro basement-involved fold.

[12] Growth strata that are folded above the propagating tip of the Yoro thrust consist of alternating coarse-grained gravel, sand and mud of the Owari Group [*Sakamoto et al.*, 1986; *Yoshida et al.*, 1991; *Furusawa*, 1990; *Sugai et al.*, 1999b] (Figure 4). Recent analysis of cores based on lithostratigraphy, magnetostratigraphy, and tephrastratigraphy suggests that the Owari Group has been deposited during middle-late Quaternary time and contains a volcanic ash layer dated at circa 0.9 Ma in its lowest part [*Sugai et al.*, 1999b]. A 50-m-thick sequence of Holocene strata (the Nanyo Formation) overlies the Owari Group as defined by seismic profiles, borehole stratigraphy and geochronology. The uppermost section of the Nanyo Formation onlaps the eastern edge of the forelimb of the Yoro basement-involved fold and thus records its growth history during the late Holocene.

[13] The piggyback basin between the Yoro and Suzuka Mountains is filled with a 1000-m-thick sequence of alluvium that is correlated with the upper Pliocene to lower Pleistocene section of the Tokai Group in the modern Nobi basin based on lithostratigraphy and tephrostratigraphy [*Yoshida*, 1988] (Figures 8 and 9). In contrast with the modern Nobi basin, the piggyback basin unit apparently lacks middle Pleistocene to Holocene strata but is unconformably overlain, or capped by flights of late Pleistocene fluvial strath terraces. Distal alluvial channel-floodplain facies of sedimentary units in the piggyback basin are generally correlative to similar Nobi basin units except for the uppermost clastic deposits. We interpret the general

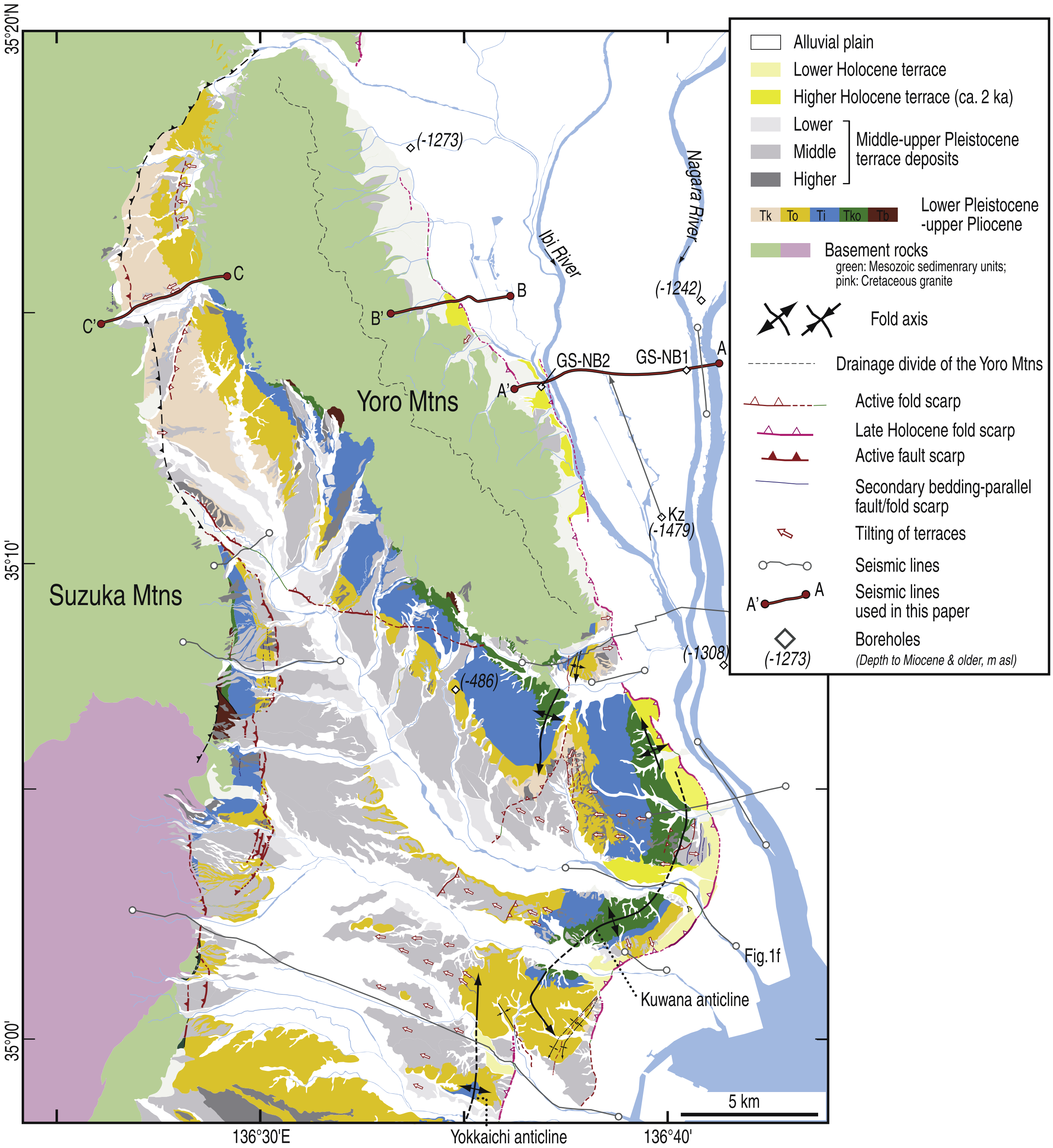

Figure 3. Geologic map of the Yoro basement-involved fold and adjacent active folds with locations of active fault and fold scarps. Geologic units are modified from *Miyamura et al.* [1976], *Takada et al.* [1979], *Yoshida* [1984, 1988], *Harayama et al.* [1989], and *Yoshida et al.* [1991]. Active folds comprise structurally and topographically elevated domains, defined by uplifted late Quaternary fluvial terraces that record structural growth since their abandonment. The location of fault and fold scarps coincides with boundaries of dip domains defined by outcrops and subsurface data. Locations of seismic sections used in this study and other lines are also shown.

correlation of strata in the Nobi basin with its now separated portion to the west as indicating that these strata are pregrowth (relative to Yoro) in nature.

4. Coseismic Fold Scarp Structure of the Yoro Thrust

4.1. Geomorphology of the Coseismic Fold Scarp

[14] The subtle, east facing scarps that offset late Holocene sediments about 5 m on the east flank of the Yoro mountains are apparent on 1:10,000 aerial photographs taken in 1940s by the U.S. military in reconstruction era Japan and modern 1:2,500 scale topographic maps [*Togo*, 2000] (Figure 10). Detailed mapping of the fold scarp at Shizu based on a 1-m-grid digital surface model (DSM) generated by photogrammetry using stereopairs taken in the 1960s prior to recent urbanization suggests that the scarps separate higher and lower Holocene terraces from the modern alluvial plain (Figure 11) [*Kawabata and Ishiyama*, 2006]. Whereas the extensive higher Holocene terrace gently dips eastward at its eastern end, a remnant of the lower Holocene terrace is subhorizontal. These two terraces are separated by east facing scarps. The sinuous trace of the scarps and a flat surface of lower Holocene terrace suggest that the scarp can be interpreted as a terrace riser made by lateral migration of alluvial rivers, rather than by artificial modification or cultivation.

[15] Boreholes A and B drilled at the base of the forelimb indicate that the folded strata underlying the surface scarps record 14 m of vertical separation as measured from the top of middle Holocene prodelta (bottom set) deposits that were presumably deposited on a near-horizontal bay (Figure 12) [*Togo*, 2000]. The prodelta unit thickens eastward by about 12 m beneath the fold scarp. In addition, overlying delta and floodplain deposits that thicken eastward by about 3 m are also folded by about 3 m of offset. We thus interpret this late Holocene topographic scarp as indicating a recent active folding event with ~3 m of vertical structural relief after middle Holocene time beneath the fold scarp (Figure 10).

[16] Late Holocene fold scarps that deform coastal plain deposits by 3–5 m are traced continuously along the leading edge of the NIFZ, including the Kuwana and Yokkaichi anticlines [*Awata and Yoshida*, 1991; *Togo*, 2000; *Ikeda et al.*, 2002; *Ishiyama et al.*, 2002a, 2004]

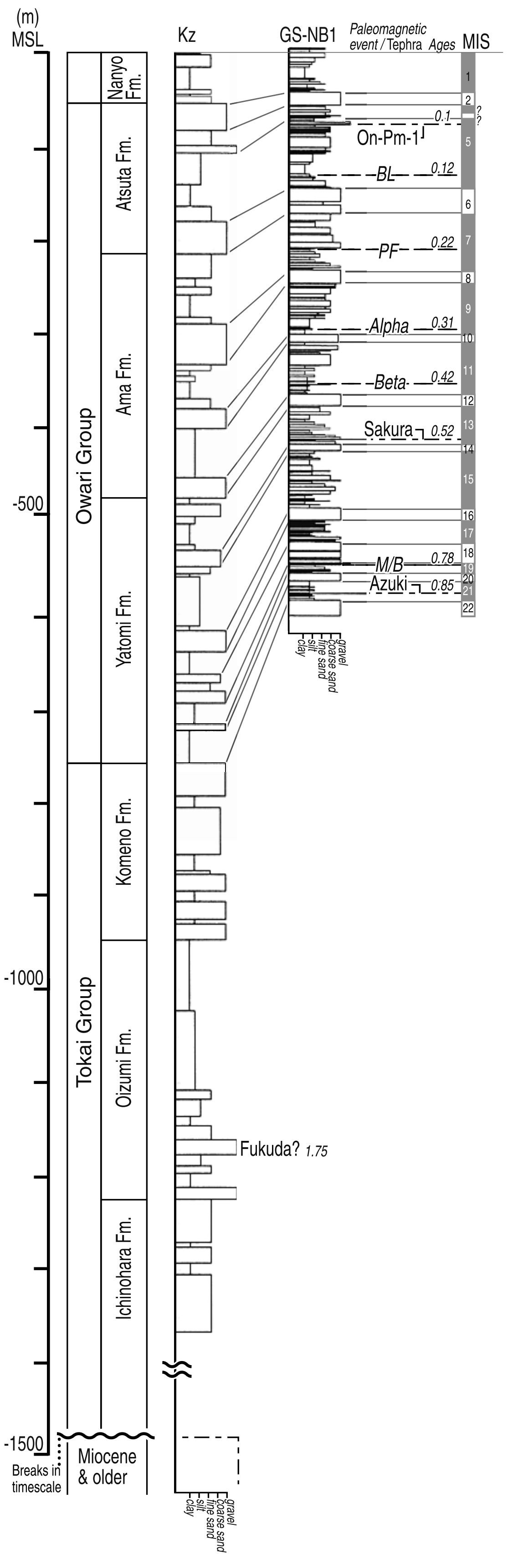

Figure 4. Borehole stratigraphy of Kz and GS-NB1 drilled in the Nobi basin with approximate ages of deposits based on lithostratigraphy, magnetostratigraphy, and tephrostratigraphy and dating by the fission track method. Rightmost column shows marine isotope stages abbreviated as MIS. Solid lines indicate correlation between cores. Dashed lines indicate paleomagnetic excursions, and chained lines indicate volcanic tephra recognized in GS-NB1 [*Sugai et al.*, 1999b]. Ages of paleomagnetic events and volcanic tephras are from *Glen and Coe* [1997] and *Machida and Arai* [2003], respectively. Other abbreviations are BL, Blake event; PF, Pringle Falls event; M/B, Matsuyama/Brunhes boundary. Unnamed Miocene (?) strata are recognized only by borehole data in the Nobi basin and are not exposed within Yoro basement-involved fold. Locations of boreholes are shown in Figure 3.

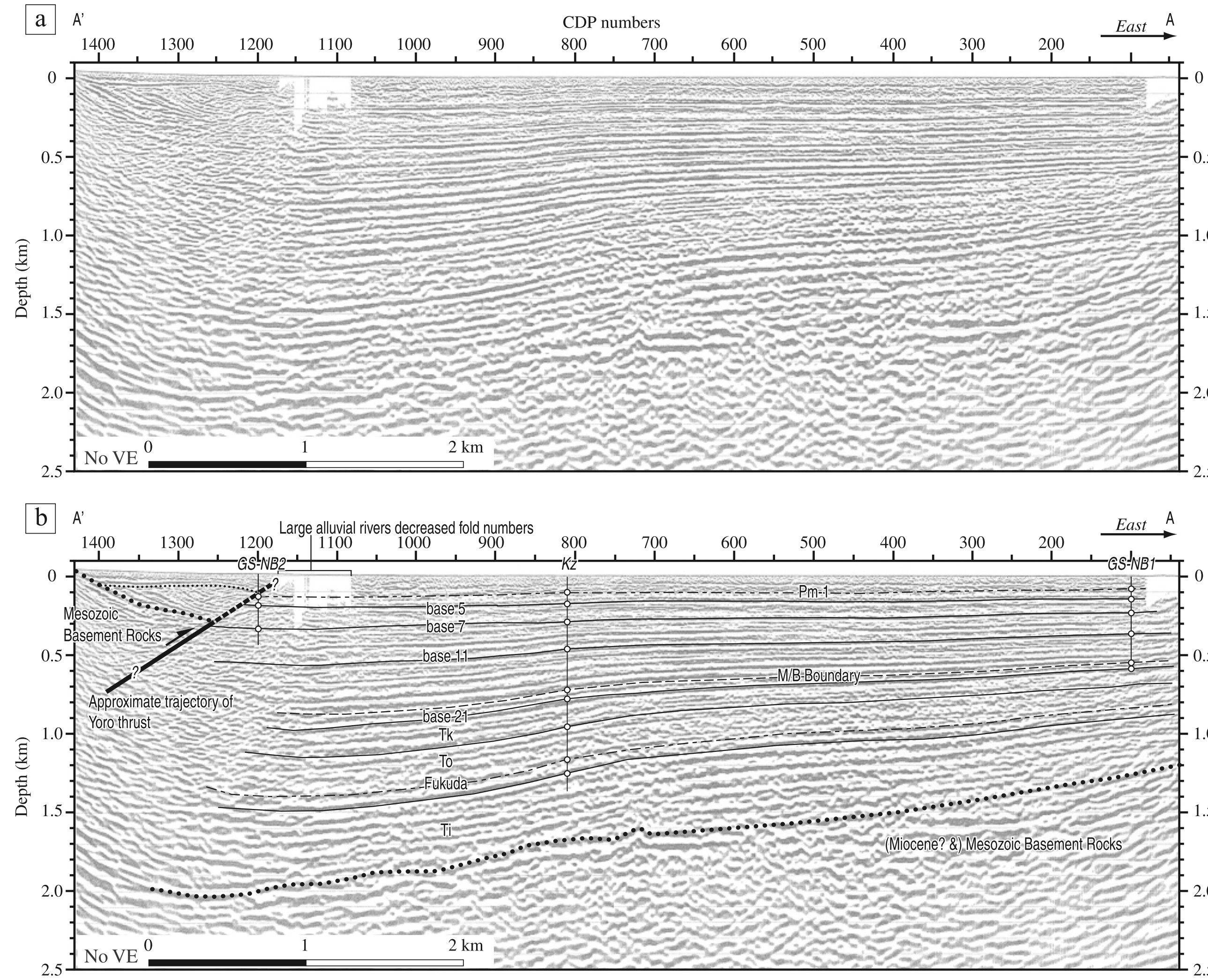

Figure 5. (a) Uninterpreted and (b) interpreted, depth-migrated seismic reflection profiles A-A' (see location in Figure 3) (modified from *Sugai et al.* [1999b]). Reflectors are correlated with borehole stratigraphy projected onto the section. Abbreviations are Pm-1, On-Pm-1 volcanic ash; Fukuda, Fukuda volcanic ash; base 5, 7, 11, and 21, base of units correlated with MIS stages 5, 7, 11 and 21, respectively; M/B, Matsuyama/Brunhes boundary; Tk, Komeno Formation; To, Oizumi Formation; and Ti, Ichinohara Formation.

(Figure 3). On the basis of tectonic geomorphology and structural analysis constrained by high-resolution seismic data, a historic earthquake that occurred on the Kuwana blind thrust system in A.D. 1586 (Tensyo earthquake M∼7.7 [*Usami*, 2003]) is shown to have produced coseismic surface deformation above both of the stacked, doubly vergent wedge tips [*Ishiyama et al.*, 2004] that define that part of the NIFZ (Figure 1f).

4.2. *S* Wave Seismic Reflection Data Beneath the Coseismic Fold Scarp

[17] In an effort to define the detailed subsurface geometry of the fold scarp, we acquired shallow high-resolution seismic reflection data across the coseismic fold scarp at Shizu (Figure 12; location of the seismic line is shown in Figure 10a). An S wave vibrator source and 1-m spacing geophones designed for S wave detection were used for the data collection. Reflectors imaged on the seismic profile were tied with strata defined in boreholes in the modern Nobi basin [*Ishiyama et al.*, 2002b; *Nakanishi*, 2003] (see their locations in Figures 10 and 12). Very strong (i.e., high-amplitude) and continuous reflectors lie about 40 m below the ground surface in the basin near the southwest end of the section. The uppermost of these prominent reflectors is interpreted as the top of late Pleistocene alluvial fan deposits that are exposed west of the Shizu area (Figure 10). Radiocarbon dating suggests that the age of this stratigraphic horizon is about 15.5 ± 1.2 ka [*Nakanishi*, 2003].

[18] The prominent reflectors tied with the alluvial fan deposits in the boreholes are clearly folded beneath the east facing fold scarp as indicated by the seismic profile (Figure 12b). Subhorizontal reflectors in the syncline to the northeast are continuous with reflectors in the forelimb (Figure 12b). These strata collectively define a distinctive

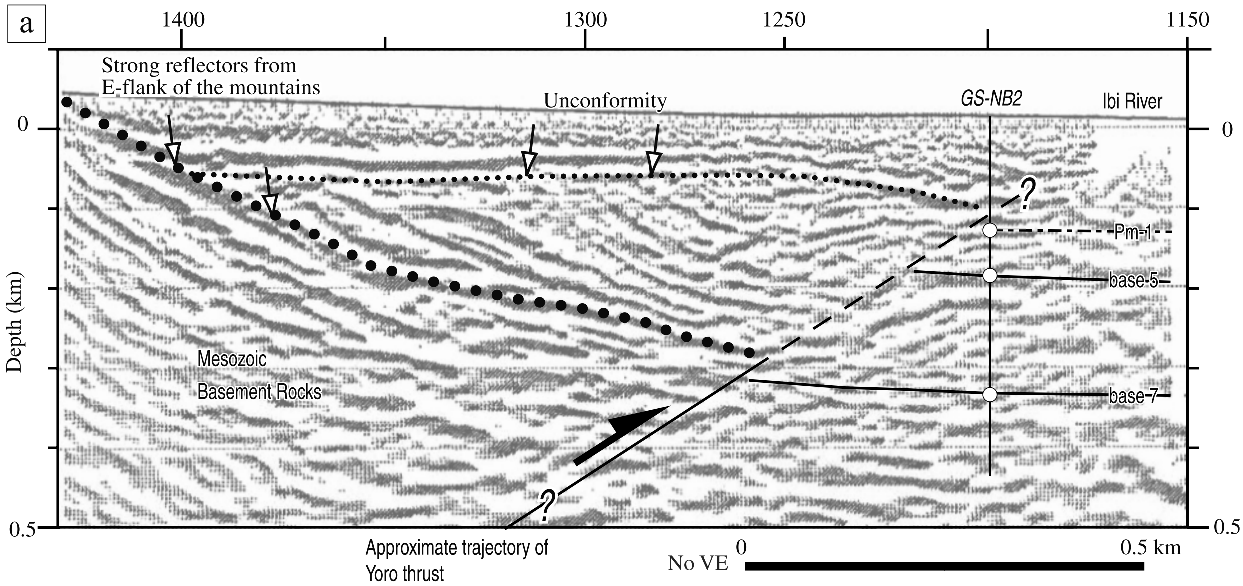

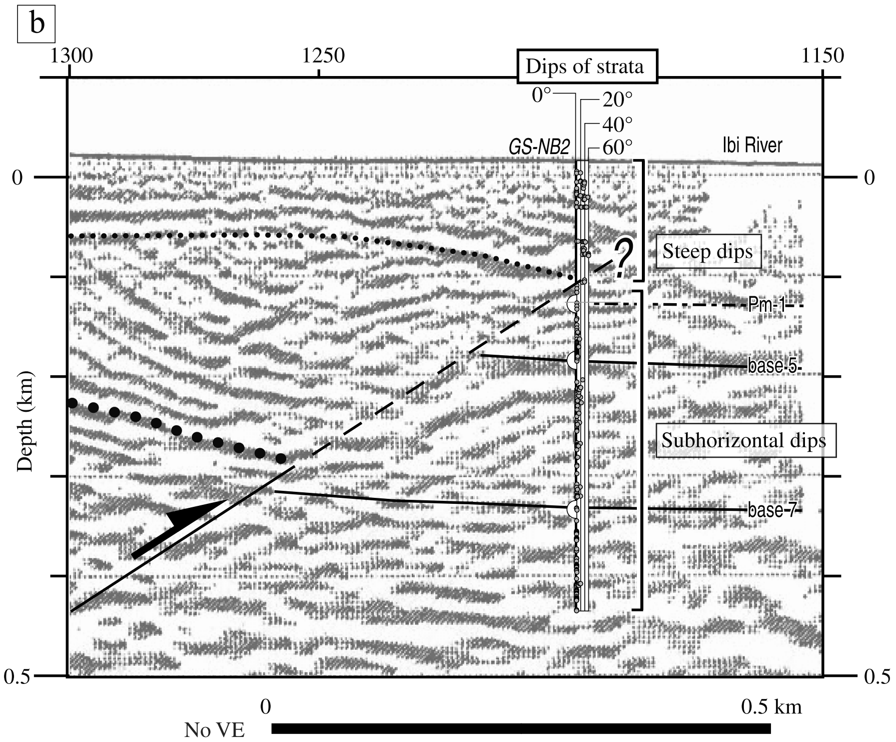

Figure 6. (a) Enlarged, detailed interpreted seismic section same as shown in Figure 5. East dipping strong reflectors traced from the western end of the seismic line are from the eastern flank of the Yoro Mountains forming the forelimb of the Mesozoic basement-involved fold. These strong reflectors from the basement rocks are underlain by a subhorizontal reflection correlated with the base of fluvial deposits during MIS 7, indicating a reverse fault that offsets strata at the base of the forelimb. (b) Deep borehole GS-NB2 [*Sugai et al.*, 1999b] drilled on the forelimb of the basement-involved fold showing that the random dip domain is underlain by subhorizontal dip domain dominant below a depth of about 100 m, interpreted as an upward projection of a thrust fault.

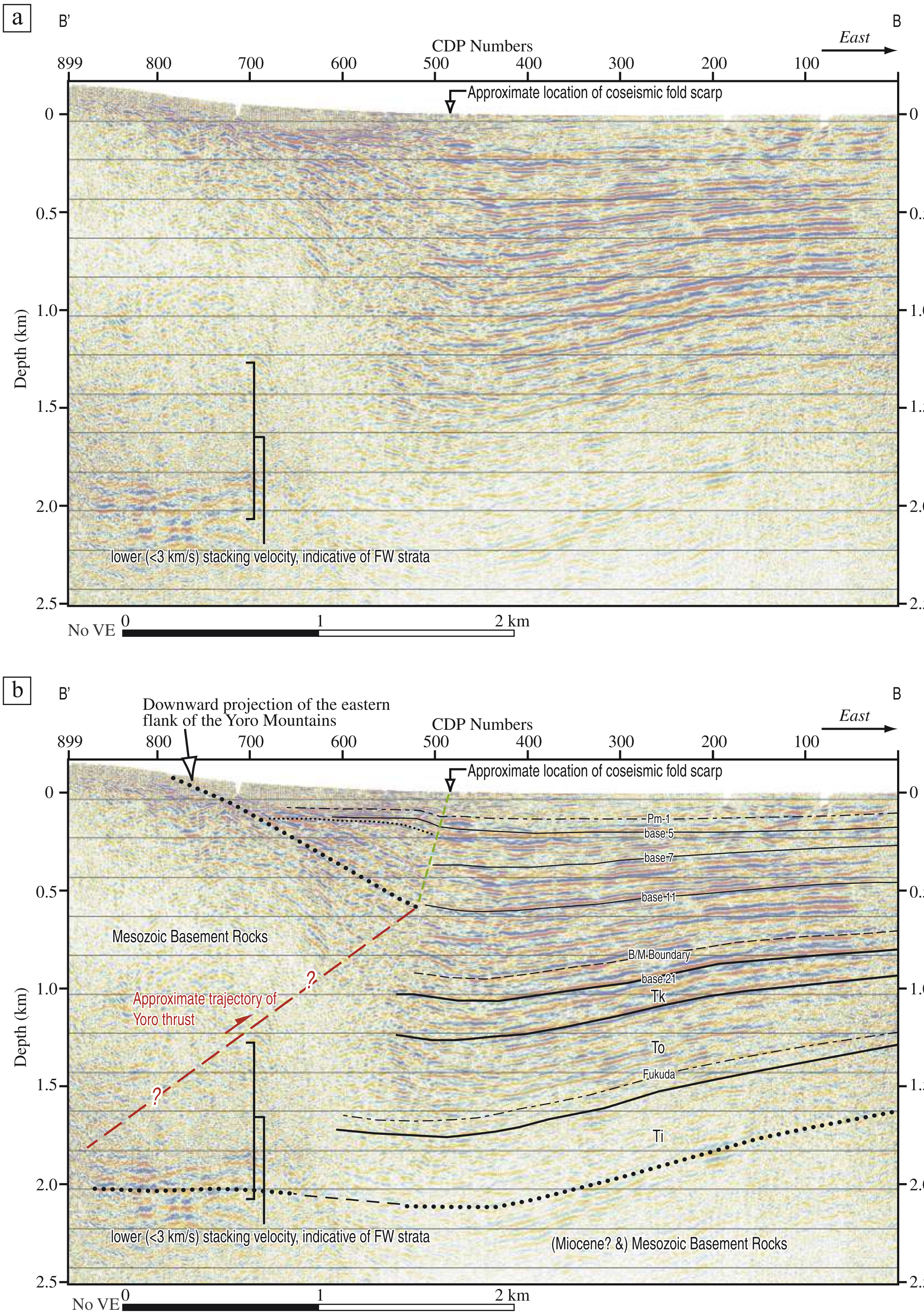

Figure 7. (a) Uninterpreted and (b) interpreted depth-migrated seismic profile across the forelimb of the Yoro basement-involved fold acquired for this study. Location is shown on Figures 3 and 10. No vertical exaggeration. Reflectors are correlated with those in A-A' tied with borehole stratigraphy. Abbreviations are the same as Figure 5. Note that trajectory of the Yoro thrust for the highest level in is a preliminary one and discussed in section 5.5.

synclinal axial surface that bisects the interlimb angles, rather than a reverse fault that offsets strata at the base of the forelimb.

4.3. Shallow Structure of the Coseismic Fold Scarp

[19] We also acquired 21 cores up to 5 m long using a "Geoslicer" [*Nakata and Shimazaki*, 1997; *Atwater et al.*, 2001] and 15 cores up to 7 m long using a percussion core sampler in an east-west transect along the high-resolution seismic line across the fold scarp at the same site [*Ishiyama et al.*, 2002b] (Figures 12, 13, and 14). Boreholes and Geoslicer panels penetrated a late Holocene sequence of delta front (foreset) sand deposits, overlying peaty clay, sandy silt, and sandy clay (top set and alluvial plain) deposits above a (bottom set) prodelta unit penetrated by deeper boreholes A, B and C (Figure 12). While sandy foreset and peaty clay deposits (lower section of unit 2) are laterally continuous and can be traced along the entire 500-m length of the transect, sandy silt (uppermost unit 2) and muddy silt deposits (unit 1) are located only beneath the higher and lower Holocene terraces (Figure 14). Radiocarbon dating of 18 samples obtained from the cores shows that sediment accumulation has been continuous during the past 10,000 years with no major depositional hiatus (Table 1) [*Ishiyama et al.*, 2002b], as indicated by *Nakanishi* [2003].

[20] Near-surface stratigraphic relations, radiocarbon dating and structural restoration of folded strata point to late Holocene and historic fold growth events at this site. Among the events are two recent earthquakes that postdate deposition of the peat layer (A.D. 120–660) in unit 2. The most recent event occurred in historical time, as suggested by offset of floodplain deposits (unit 1). Considering that unit 1 is composed of alluvial river channel/floodplain sandy mud deposits interbedded with flat-lying thin sand layers just beneath the lower Holocene terrace, the lower Holocene terrace is interpreted as a depositional surface of unit 1 at the time of river incision discussed later. Although it is not possible to correlate unit 1 across the frontal scarp along the bank, we interpret unit 1 as comprising both the lower Holocene terrace and alluvial plain deposits based on their uniform lithology and similar ages (Figures 13 and 14). A 2.3-m relief across the top of unit 1 thus records an uplift event after deposition of unit 1 rather than strata draped above an existing fold scarp. The uppermost section of unit 1 contains historical material dated by radiocarbon methods (A.D. 1446–1695) that underlie the lower Holocene terrace (Figure 7). We therefore argue that this uplift episode occurred in historical time and can be correlated with the Tensyo earthquake in A.D. 1586 [*Usami*, 2003].

[21] A penultimate uplift event may be suggested by folding of unit 2 beneath the higher alluvial plain. Unit 2 composed of sandy delta front (foreset) deposits and overlying peat and sandy silt deposits are gently inclined, similar to the slope of the higher Holocene terrace. Peaty clay within unit 2 is more deeply buried and thicker at the base of the frontal fold scarp (i.e., the topographic boundary between the lower Holocene terrace and modern alluvial plain) and is folded into a more steeply dipping panel located near the base of the fold scarp. We thus interpret that an uplift event occurred after deposition of unit 2 (A.D. 120–389) and before deposition of unit 1 (A.D. 1021–1155). This possible paleoseismic event may be correlated with a documented earthquake in A.D. 745 (Tenpyo earthquake M$\sim$7.9 [*Usami*, 2003]). We distinguish this event from the most recent historic event because (1) structural relief of unit 2 is almost 5 m, about twice that of unit 1, and (2) flat-lying strata of unit 1 onlap the lower section of east dipping unit 2 near the topographic boundary between the Holocene terraces above a buttress unconformity expressed by a sharp contact and an overlying thinly bedded coarse-grained sand and gravel layer, respectively. A buttress unconformity between unit 1 and 2 is consistent with a terrace riser between the lower and higher Holocene terrace composed of unit 1 and 2. Radiocarbon age determinations of the base of unit 1 (A.D. 1021–1155) obtained just above the unconformity is approximately contemporaneous with a regional sea level fall event found at several sites in the Nobi basin [*Umitsu*, 1994], suggesting that the terrace riser and buttress unconformity resulted from a change in base level associated with a fall in regional sea level. Our paleoseismic interpretation of two historic (i.e., Tensho and Tenpyo) earthquakes is consistent with results at other sites along the Yoro fault [*Sugai et al.*, 1999a] and the Kuwana fault [*Sugai et al.*, 1998].

[22] Although the geometry of a stratigraphic unit between the prodelta (bottom set) unit and unit 2 is not defined in detail by this study, larger structural relief measured across the prodelta unit (14 m) in relation to that of unit 2 (5 m) can be interpreted to indicate at least one uplift event after deposition of the prodelta unit at 5.3 ka [*Nakanishi*, 2003] and before the end of deposition of unit 2, prior to the two recent earthquakes.

[23] The geometry of folded alluvial fan deposits imaged by the S wave seismic reflection data is consistent with near-surface late Holocene and historic deposits in that the upward projection of the synclinal axial surface at the base of the forelimb that deforms alluvial fan deposits coincides with the base of the coseismic fold scarp (Figure 12). In addition, the steeper forelimb and gentler backlimb are also apparent both at the ground surface and in late Holocene deltaic deposits. We therefore argue that the topographic scarp at this site was produced by discrete active folding associated with repeated large earthquakes on the blind Yoro thrust during the Holocene, including the historic A.D. 1586 earthquake.

5. Deeper Subsurface Structure of the Yoro Basement-Involved Fold

5.1. Seismic Reflection Data

[24] Reflectors on an existing seismic reflection profile A-A' obtained in the Nobi basin were correlated with strata defined by two deep boreholes in the vicinity of, and about 7 km southeast of the seismic line with stratigraphic contacts of known age [*Sugai et al.*, 1999b] (Figure 5, see its location in Figure 3). Lithologic changes (i.e., alternation of sandstone and mudstone) defined in the boreholes are also consistent with phase changes in seismic reflectors [*Sugai et al.*, 1999b], which also supports the stratigraphic correlations made in our analysis. Continuous, high-amplitude reflectors are imaged 1500 m below the ground surface at the eastern end of the seismic section, which are interpreted as the late Pliocene to early Pleistocene Tokai Group,

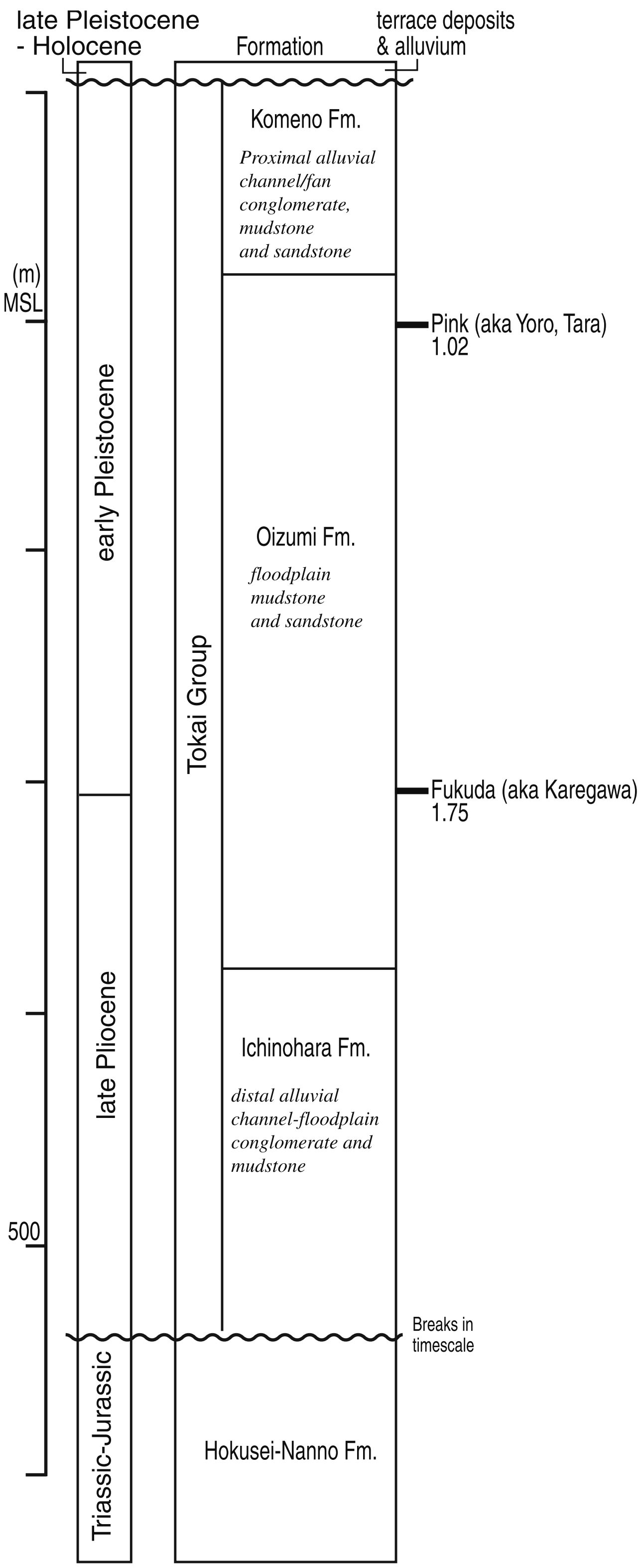

Figure 8. Stratigraphic column of piggyback basin between the Yoro and Suzuka Mountains, with approximate ages of deposits based on tephrochronology and dating by the fission track method [*Yoshida*, 1988].

middle to late Pleistocene Owari Group and Holocene Nanyo Formation.

[25] Another important observation of strata imaged in the footwall syncline of the Yoro thrust includes the presence of subparallel, gently west dipping beds of Plio-Pleistocene Tokai Group with uniform thickness of 700 m that are overlain by westward thickening beds of Owari Group that flatten upward with decreased depth of burial (Figure 5). We interpret this to indicate that reflectors correlated with the Tokai Group were deposited prior to uplift of the basement-involved fold. Additional evidence for the pregrowth nature of these strata includes their consistent stratigraphic thickness with correlative units exposed on the backlimb of the Yoro basement-involved fold in the piggyback basin to the west.

[26] Correlation of reflectors with boreholes GS-NB1 and GS-NB2 [*Sugai et al.*, 1999b] indicate that strong reflectors from the basement rocks are underlain by a subhorizontal reflector correlated with the base of fluvial deposits during Marine Isotope Stage (MIS) 7, suggesting that a reverse fault offsets strata at the base of the forelimb (Figure 6). However, despite the good correlation of reflectors with borehole stratigraphy, section A-A' does not resolve Pleistocene-Holocene strata in enough detail to compare the geometry of the relatively narrow coseismic fold scarps with older growth architecture. This resulted from the locations by wide alluvial rivers, which limited the placement of certain source points during acquisition of the seismic profile, resulting in lower stacking of traces near the fold scarp. In addition the forelimb and footwall near the underlying thrust are poorly imaged because the seismic line ended in the middle of the forelimb. These issues motivated acquisition of new continuous and closely spaced seismic reflection profiles.

5.2. Acquisition of New Seismic Reflection Data

[27] Two high-resolution seismic reflection profiles across the forelimb (B-B'), and the backlimb of the Yoro basement-involved fold and the forelimb of the Ichishi basement-involved fold (C-C') were thus acquired as a part of this study to further image its subsurface geometry. We used the multichannel recording system and a seismic source (minivibrator) of the Earthquake Research Institute, University of Tokyo (Figures 7 and 9; see locations in Figure 3 for B-B' and C-C'). A 180-channel recording system GDaps-4 was used in an off-end configuration with the nearest receiver adjacent to the source to record seismic waves from deeper reflection points. A 10-m source and geophone spacing was used and gives a 5-m common depth point (CDP) spacing on the final section B-B' and C-C'. The nominal CDP stacking fold was 90 traces for B-B' and C-C'. We also increased the stacking fold by repeating source points 5–10 times.

[28] Data processing was routine for seismic reflection data [cf. *Yilmaz*, 1987], including surface-consistent statics by use of refractors, velocity analysis based on Normal moveout (NMO) method and residual statics, and the sections were finally depth-converted by use of stacking velocities. Reflectors imaged on the seismic profile were tied with strata defined in boreholes in the Nobi basin [*Sugai et al.*, 1999b] (see their locations in Figure 3), stratigraphic contacts on the geologic maps, and volcanic

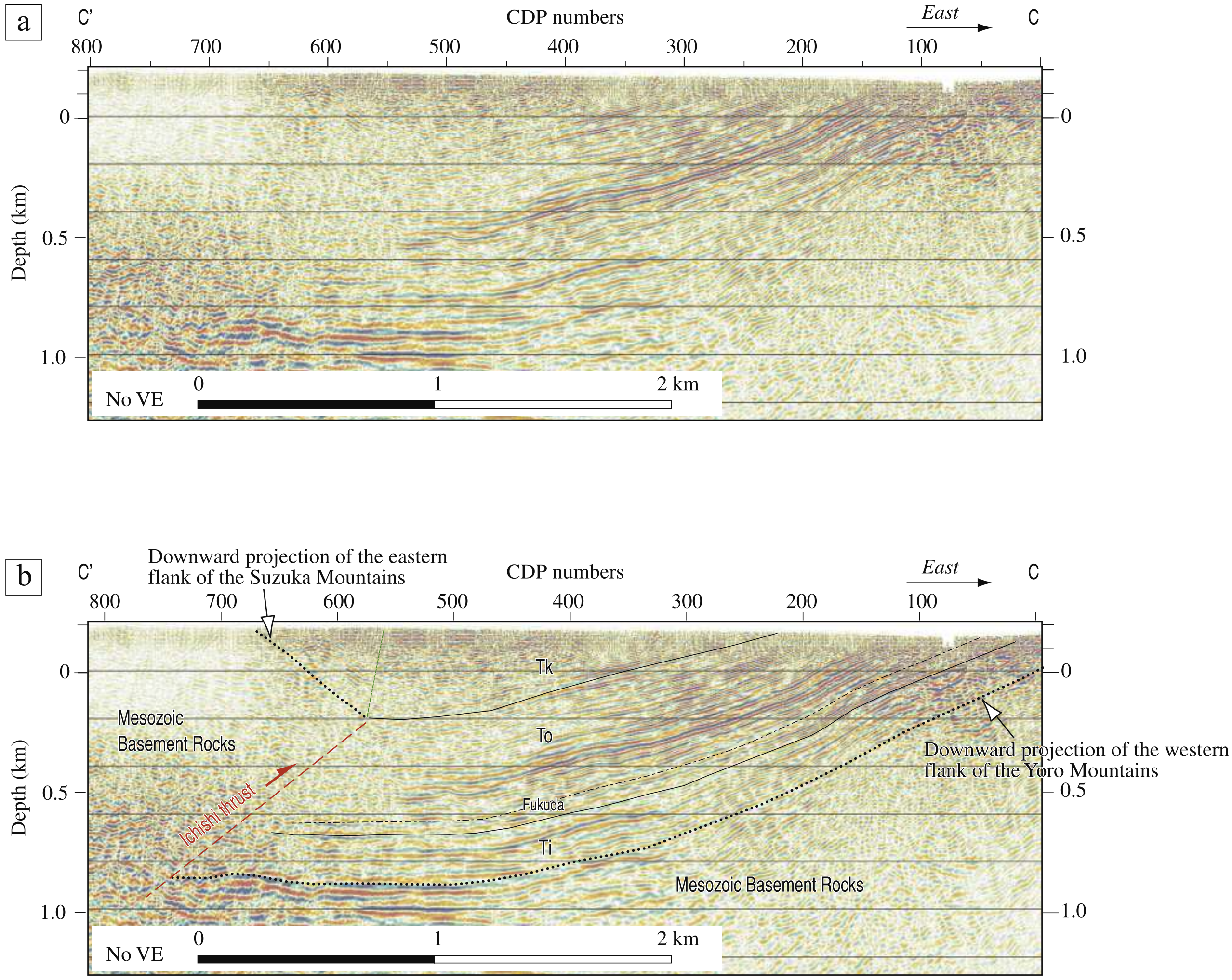

Figure 9. (a) Uninterpreted and (b) interpreted depth-migrated seismic profile across the piggyback basin west of the Yoro basement-involved fold acquired for this study. Location is shown on Figure 3. No vertical exaggeration. Reflectors are correlated with geologic mapping shown in Figure 3. Abbreviations are the same as Figure 5.

tephra exposed on the backlimb of the Yoro basement-involved fold and the forelimb of the Ichishi basement-involved fold.

5.3. Forelimb Structure of the Yoro Basement-Involved Fold

[29] Reflectors in the footwall of the Yoro thrust in the section A-A' were tied with strata defined in section 5.2 (Figure 5) projected onto a vertical plane perpendicular to the surface trace of fold scarps. Similar to section 5.2, prominent reflectors of uniform thickness in the footwall syncline of the Yoro thrust are interpreted as the Tokai Group (Figure 7). These are overlain by westward thickening strata of the Owari Group that lie 1000 m below the ground surface at the eastern end of the section. On the upraised part of the fold, east dipping, high-amplitude reflectors with lower interval velocities (less than 3.0 km/s) are evident above discontinuous reflectors with lower frequencies and higher interval velocities (more than 3.0 km/s). Upward projection of the deepest east dipping high-amplitude reflectors suggests that they correspond to Jurassic-Mesozoic basement rocks that form the core and forelimb of the basement-involved fold. We thus interpret these high-amplitude reflectors with lower velocities and underlying, lower amplitude reflectors as Pliocene-Pleistocene strata originally deposited in the Nobi basin and the basement rocks respectively, which now are incorporated into the forelimb of the fold.

[30] The oldest rocks deformed in the forelimb of the Yoro basement-involved fold include east dipping Pliocene-Pleistocene strata of consistent thickness that are parallel to the underlying basement rocks. Pliocene-Pleistocene strata are deformed evenly by the forelimb suggesting that they were deposited prior to uplift of the fold and thus are pregrowth strata. In addition, unconformably overlying middle Pleistocene and younger units thin across the east dipping forelimb, suggesting that they were deposited concurrent with fold growth and fault activity. An angular unconformity between Pliocene and younger units is also apparent on the forelimb as previously noted by A-A' (Figures 5 and 6). Most importantly, this Quaternary growth architecture exhibits an active synclinal axial surface that

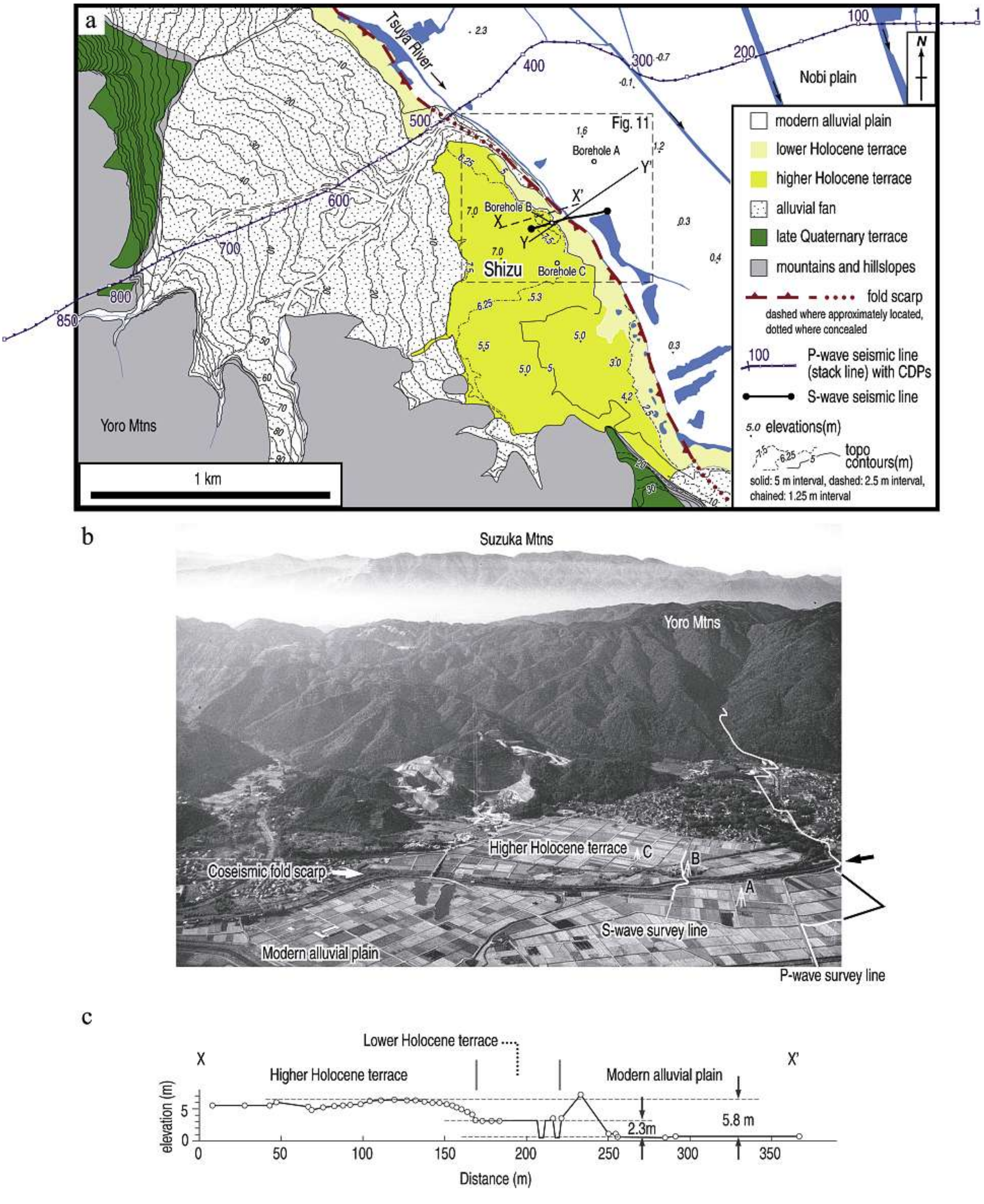

Figure 10. (a) Detailed topography of the forelimb of the Yoro basement-involved fold (modified from *Ishiyama et al.* [2002b]). Topographic map with 2-m contour interval is redrawn from 1:3,000 topographic maps. East verging small fold scarps at the base of the forelimb that deforms late Holocene units are identified. (b) Oblique aerial view of the eastern flank of the Yoro Mountains. Small fold scarp locates at the base of the forelimb of the Yoro basement-involved fold. Low-relief topography at the top of the Yoro Mountains indicates relict erosional surface formed as unconformity between Mesozoic basement rocks and Pliocene strata. (c) Topographic profile across the entire extent of the fold scarp.

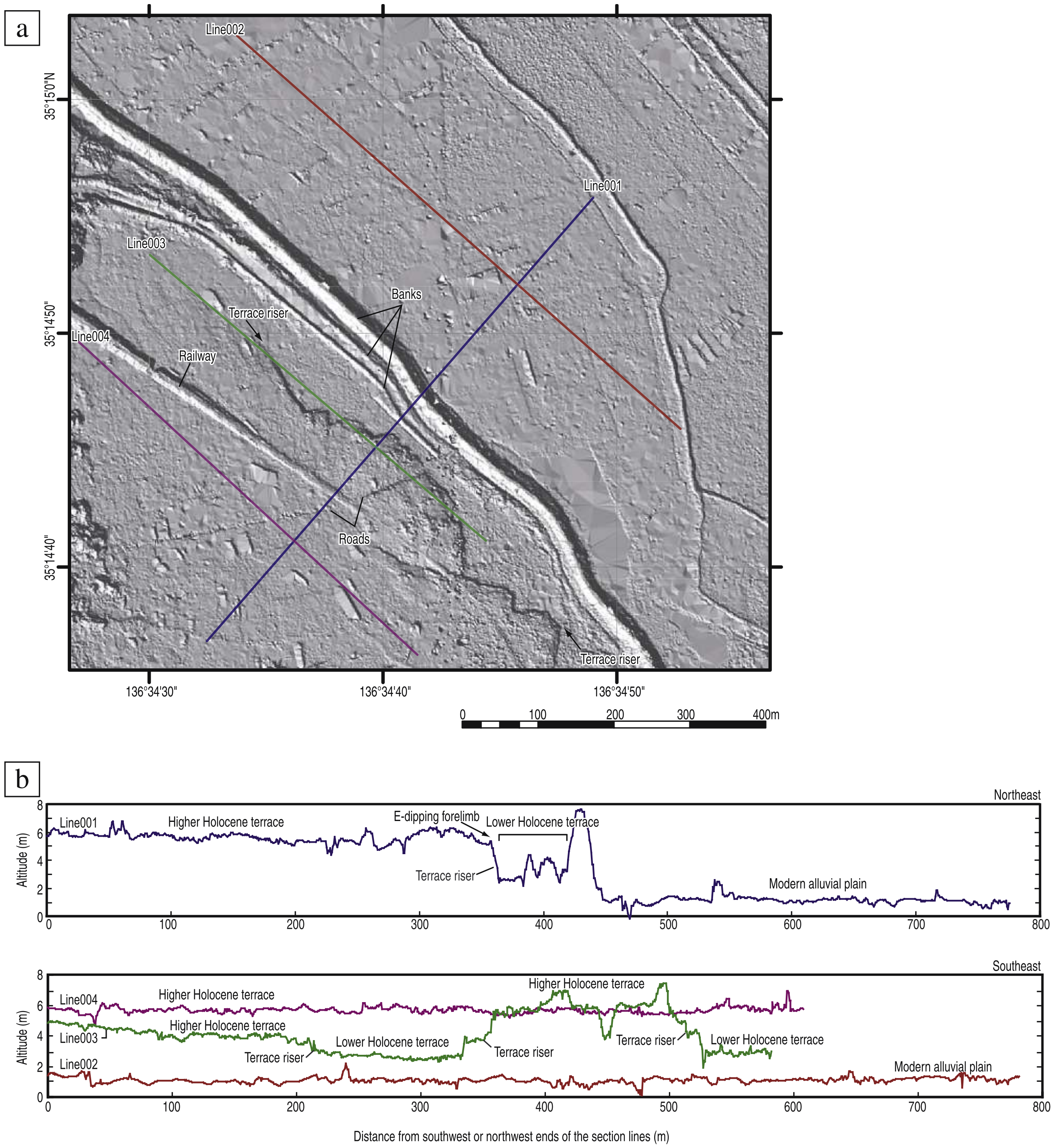

Figure 11. (a) Shaded relief image of the fold scarp of the Yoro basement-involved fold at Shizu, based on 1-m grid, photogrammetric digital surface model using stereopairs taken in 1961 [*Kawabata and Ishiyama*, 2006]. (b) Topographic profiles taken in both the along- and cross-strike direction of the fold scarp. Sinuous traces of terrace risers that separate the higher Holocene terrace from a lower Holocene terrace are distinctively shown. Lower Holocene terrace is also separated from modern alluvial plain by a 2-m-high topographic scarp.

extends to the base of the coseismic fold scarp (Figure 7b). This is diagnostic of a wedge thrust structure [*Medwedeff*, 1992] and implies growth by the mechanism of kink band migration [*Suppe et al.*, 1992] above an active wedge tip [*Ishiyama et al.*, 2004] or a fault propagation fold [*Suppe and Medwedeff*, 1990; *Erslev*, 1991; *Hardy and Ford*, 1997; *Allmendinger*, 1998]. Forelimbs defined by shallowly inclined dip domains and sharply angular interlimb angles are, however, inconsistent with mechanisms of fault propagation folding. We therefore interpret the Yoro basement-

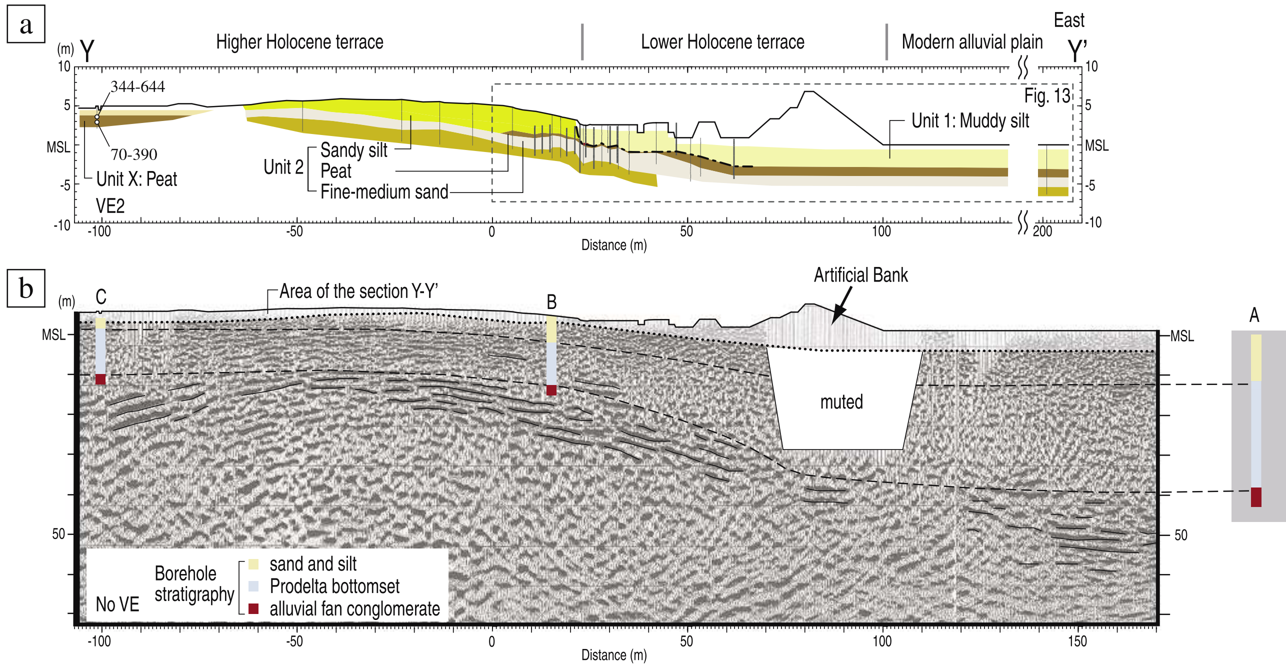

Figure 12. (a) Geologic cross section across the fold scarp of the Yoro fault near Shizu based on Geoslicers and drilled boreholes (modified from *Ishiyama et al.* [2002b]). (b) A high-resolution S wave seismic reflection profile (depth migrated) across the coseismic fold scarp. Boreholes tied with prominent reflectors are also shown. Stratigraphy of the borehole B is identified by *Nakanishi* [2003]. Locations of the cross section, seismic section, and boreholes are shown on Figure 10a.

involved fold as forming as an east vergent wedge thrust structure. Below the eastern flank of the Yoro Mountains, subhorizontal, continuous and strong reflectors with low frequencies lie beneath poorly defined reflectors visible at depth of 1700–2000 m between CDP 700 to 880 in the seismic section (Figure 7). Interval velocities of these reflectors (less than 3.0 km/s) are apparently lower than the Jurassic-Triassic strata deformed in forelimb of the basement-involved fold. Therefore we interpret the prominent reflectors with lower velocities as corresponding to lowermost Tokai Group strata that are also identified in the Nobi basin, and hence that the thrust wedge involves Jurassic-Triassic basement rocks that have been thrust over younger deposits in the Nobi basin.

5.4. Backlimb Structure of the Yoro Basement-Involved Fold and Piggyback Basin

[31] Seismic reflection profile C-C' located in the piggyback basin between the Yoro and Suzuka Mountains images Jurassic and Triassic strata that forms the core of the Ichishi basement-involved fold and are thrust over late Pliocene

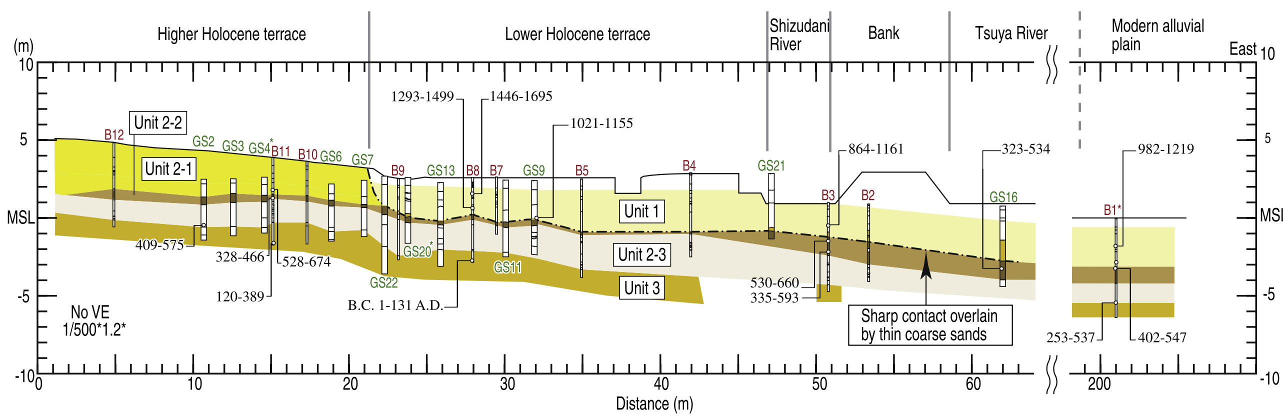

Figure 13. Enlarged geologic cross section across the fold scarp of the Yoro fault near Shizu based on Geoslicers and drilled boreholes (modified from *Ishiyama et al.* [2002b]). Sharp contacts between unit 2-2 and unit 1 beneath the lower Holocene terrace are often marked by medium to coarse sands with gravels, in orange. Ages are calendric and calibrated as shown in Table 1. No vertical exaggeration. Detailed lithologic description of cores marked by asterisks is shown in Figure 14.

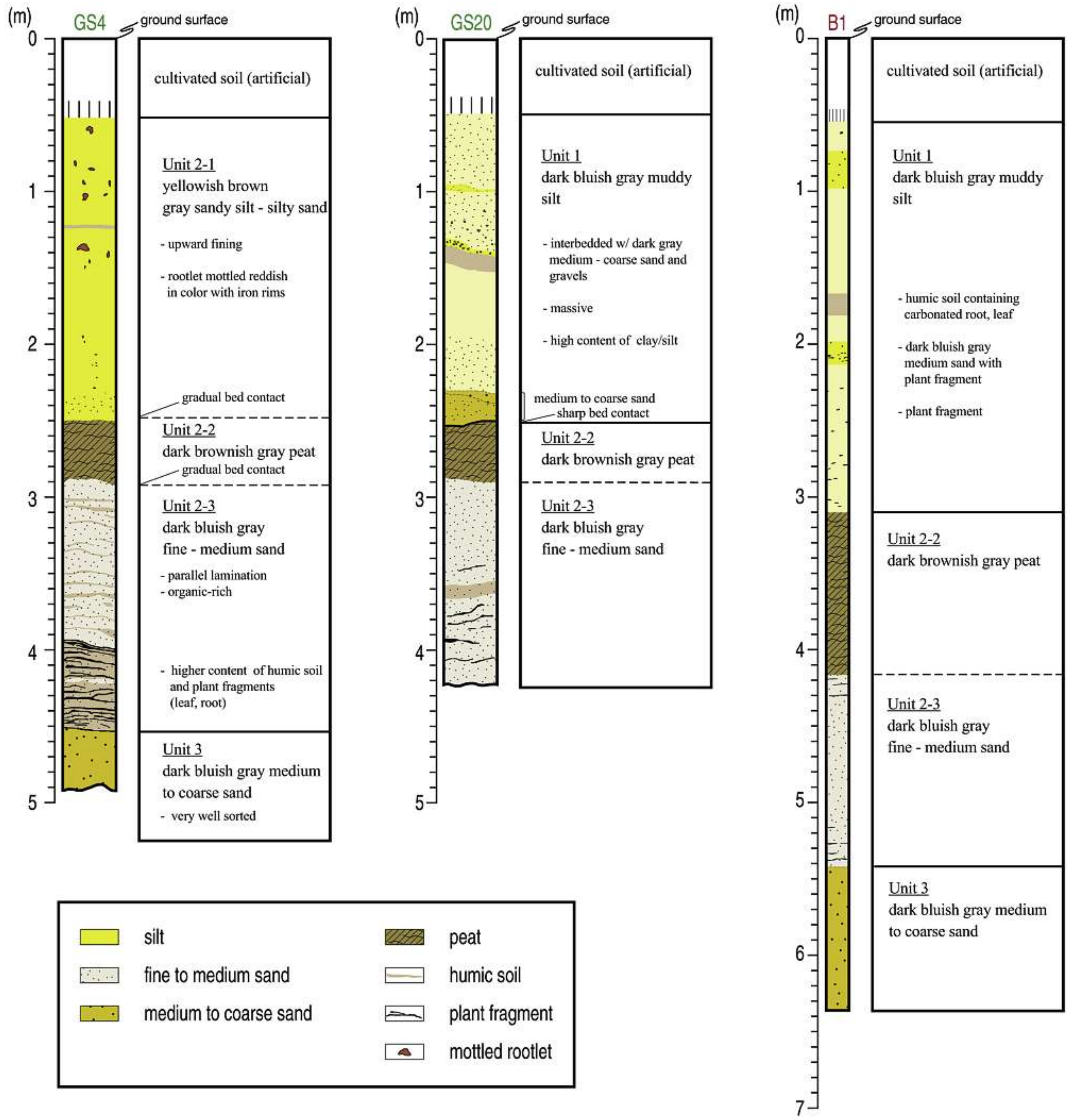

Figure 14. Stratigraphic columns of units obtained at points in higher and lower Holocene terraces (GS4 and GS20) by Geoslicer and in modern alluvial plain (B1) by a percussion sampler (modified from *Ishiyama et al.* [2002b]). Lithologic description of units is also shown.

and early Pleistocene strata (Figure 9). Footwall stratigraphic cutoffs imaged in the seismic section beneath the forelimb of the Ichishi basement-involved fold indicate that it is underlain by a shallowly (38°) west dipping thrust fault. Continuously traced horizons within the uppermost Tokai Group (Komeno Formation) across the synclinal axial surface at CDP 560 suggest that strata are folded across the synclinal axial surface extending from the upper tip line of the Ichishi thrust, rather than being cut by a thrust fault as is more typical for much of the NIFZ.

[32] A 800-m-thick section of Pliocene and early Pleistocene strata does not change thickness across the backlimb of the Yoro basement-involved fold, also suggesting that these sediments were deposited prior to fold growth. The pregrowth nature of strata deposited in the piggyback unit is also defined by (1) correlative, 800-m-thick, lowermost Nobi basin units that do not change thickness across the Yoro structure and (2) the projection of an unconformity between the Pliocene-Pleistocene piggyback units and Mesozoic basement rocks imaged in C-C’, which is contin-

Table 1. AMS Radiocarbon Dates of Materials Sampled From Cores by Geoslicers and Percussion Samplers[a]

Laboratory Code[b]	Dated Material	^{14}C Ages Conventional; 1σ, years B.P.	δ^{13}C Value, ‰	Calibrated Ages Calendric, 2σ[c]	Sampled Unit*
1827	plant fragment	276 ± 77	−27.5	1446–1695	1
1828	leaf, humic soil	507 ± 66	−27.4	1293–1499	1
1829	wood	1040 ± 66	−27.5	864–1161	1
1830	humic soil	951 ± 64	−28.3	982–1219	1
1838	humic soil	1648 ± 34	−27.7	328–466	2–2
1839	humic soil	1468 ± 52	−27.8	530–660	2–2
1840	humic soil	1600 ± 58	−27.8	335–593	2–2
1841	humic soil	1592 ± 34	−27.6	402–547	2–2
1852	humic soil	1658 ± 59	−27.1	253–537	2–3
1854	charcoal	1786 ± 58	−28.5	121–389	3
1855	charcoal, leaf	1935 ± 33	−26.4	1 B.C. to A.D. 131	3
1857	wood	1558 ± 78	−28	344–644	X
1858	plant fragment	1804 ± 70	−28.2	70–390	X
1996	charcoal	1448 ± 61	−25	528–674	2–1
Beta-129716	wood	1570 ± 40	−29.2	409–575	2–3
Beta-129717	wood	1220 ± 40	−27	685–892	2–2
Beta-129720	wood	960 ± 30	−27.4	1021–1155	1
Beta-129721	wood	1650 ± 40	−27.7	323–534	2–2

[a]Modified from *Ishiyama et al.* [2002b].
[b]Samples denoted by "Beta" were dated by Beta Analytic Inc, Miami, Florida; the other dates were measured by Japan Atomic Energy Agency (formerly the Japan Nuclear Cycle Development Institute).
[c]Conventional ages were calibrated using CALIB 5.0 [*Stuiver and Reimer*, 1993; M. Stuiver et al., CALIB 5.0., WWW program and documentation, 2005, available at http://calib.qub.ac.uk/calib/].

uous with low-relief erosional surfaces on the backlimb and crest of the fold. We thus argue that the topography of the Yoro Mountains essentially defines the shape of the stripped unconformity that is overlain by pregrowth strata of the Nobi basin (i.e., Pliocene–lower Pleistocene Tokai Group).

[33] Recent growth of the backlimb of the Yoro basement-involved fold is recorded by west dipping (i.e., upstream-inclined) fluvial terraces located in transverse channels across the eastern flank of the Suzuka Mountains. Similar to the west dipping fluvial terraces, west dipping Pliocene and early Pleistocene strata are folded and flattened in the center of the piggyback basin as marked by a synclinal axial surface. Therefore the synclinal axial surface effectively defines the backlimb of the basement-involved fold above the Yoro thrust and is interpreted to be pinned at depth to a steeper ramp at depth.

5.5. Fold Geometry and Fault Slip Budget

[34] The Yoro basement-involved fold has likely formed as a wedge thrust structure above a blind thrust that steepens upward across several gentle bends (Figure 15). Smoothed topography of the Yoro Mountains based on a 50-m digital elevation model suggests that the elevation of high mountain topography can be used as a crude proxy for the shape of the stripped unconformity between the Mesozoic basement rocks and the Nobi basin deposits (i.e., relict erosion surfaces) (Figure 16). Reconstruction of topography based on the 50-m DEM suggests that the unconformity is defined by a flat-lying dip panel on the crest of the fold and several dip domains in the forelimb and backlimb. The forelimb of the basement-involved wedge thrust fold can be further subdivided into two dip domains based on topography.

[35] Fault bend fold theory [*Suppe*, 1983] predicts that active axial surfaces separating dip panels in anticlinal bends can often be related to folding at the top of thrust ramps (Figure 15). We therefore use the dips of strata in the forelimb of Yoro (28° For the lower dip domain and 12° For the upper dip domain) and the dip of axial surfaces (84° and 76°) to develop a fault solution where a deeper thrust ramp dips 31° and flattens to 23° at higher levels across an anticlinal bend.

[36] The deepest geometry of the thrust ramp is constrained by an active synclinal axial surface as defined by folded fluvial terraces in the piggyback basin. Using the topography of the exhumed unconformity on the west flank of the Yoro Mountains and the top of the same contact in the piggyback basin as imaged by seismic data, we argue that backlimb strata are folded across two curved hinges [*Suppe et al.*, 1997; *Shaw et al.*, 2005] that mark similar fault bends at depth. On the basis of fault bend fold theory [*Suppe*, 1983], the dip of strata in the west dipping backlimb (26°) and the dip of "entry" and "exit" synclinal axial surfaces (77°) we predict that the 31° west dipping thrust ramp flattens to 5° at lower levels across a curved synclinal bend on the fault.

[37] We measured the fault slip budget upward through the Yoro basement-involved fold to test whether it grows as a wedge thrust structure, or whether other mechanisms occur that may act to control its growth (Figure 15). We first compare the width of the backlimb to the calculated values of fault slip. On the basis of a fault dip on the lower ramp of 31° and 2.6 km of vertical structural relief measured at the top of the unconformity defined by topography and constraints from seismic data, 5.0 km of fault slip has apparently been accommodated by the deeper levels of the structure. The theoretical fault slip of 5.0 km is larger than the apparent width of the backlimb (3.9 km) as defined by the distance between inactive and active axial surfaces (Figure 15). We interpret this difference to partly result because the ramp at depth is oblique to the mean fold axis. The trend of frontal active thrusts in the NIFZ and geologic mapping (Figure 3) indicates that local variation in the trend of the mean fold axis near the projection line (N148°E) may deviate from the

*The sample units are correct here. The article as originally published is online.

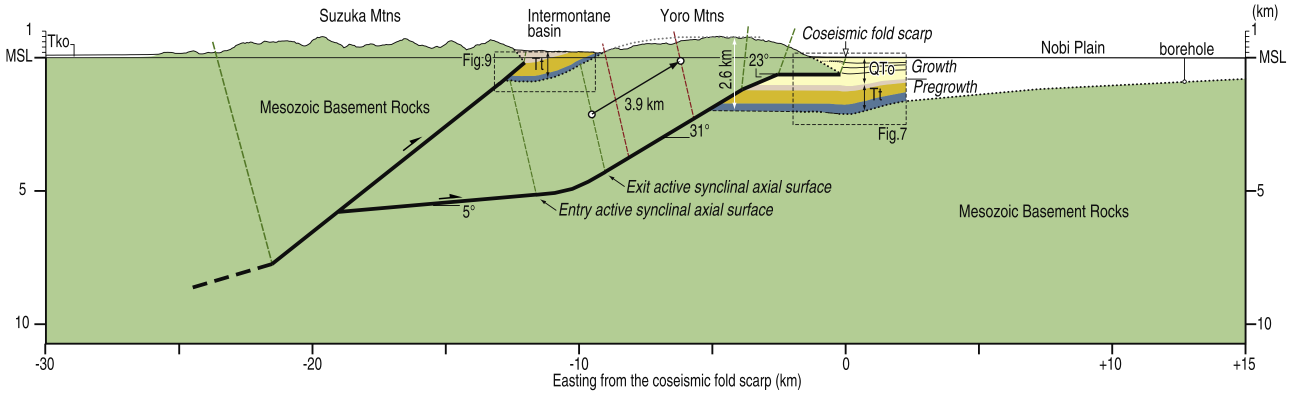

Figure 15. Geologic cross section of the Yoro basement-involved fold constrained by the seismic section, geologic mapping, and tectonic geomorphology of its forelimb and backlimb that are linked with bends on the underlying fault trajectory. The close links between the forelimb and backlimb geomorphology and the fault geometry support the wedge thrust model for Yoro basement-involved fold. Abbreviations are Tt, Pliocene-Pleistocene Tokai Group; Tko, Pliocene-Pleistocene Kobiwako Group; and QTo, middle Pleistocene-Holecene Owari Group.

regional E-W transport direction assumed for the fold. For this case, dip of the oblique ramp is defined by

$$\tan\delta' = \cos(\alpha - \alpha_0)\tan\delta$$

where δ, δ', α and α_0 are true and apparent dip of the oblique ramp, the azimuth of the local mean fold axis and of the regional mean direction of transport, respectively [*Apotria et al.*, 1992; *Groshong*, 2006]. Assuming that δ' = 31°, α = 58°, and α_0 = 90°, the true dip of the oblique ramp is calculated to be about 35°. On the basis of this more likely fault dip on the lower ramp and 2.6 km of vertical structural relief, fault slip on the ramp is calculated at this location to be about 4.5 km, which is closer to the apparent width of the backlimb than our previous estimate. We therefore suggest that at least 3.9 km of fault slip has been completely consumed by folding. In spite of the lack of surface evidence of a decollement that transfers slip further westward at higher level of the structure, we expect mechanical decoupling between sedimentary cover and underlying basement rocks on the forelimb. The forward balanced wedge thrust model is thus able to account for the bulk of the fault slip accommodated by the shallower levels of the Yoro basement-involved fold as defined by the geometry of its forelimb, further suggesting that the structure has formed as a wedge thrust fold (Figure 15).

6. Discussion

6.1. Short- and Long-Term Slip Rates of the Yoro Thrust

[38] The slip budget calculation discussed in 5.5 indicates that at least 3.9 km of fault slip has been accommodated at the deepest level of the structure (Figure 11). The age of the base of the early–late Pleistocene Owari Group interpreted as growth strata indicates that structural growth of the Yoro basement-involved fold began at about 0.9 Ma. Taking an age of 0.85 ± 0.03 Ma of volcanic ash contained in the bottom of the growth strata (Figure 4), we thus determine a dip-slip rate of 4.4 ± 0.2 mm/yr at long (10^6 years) time-scales. For the 8° lower and 23° upper anticlinal fault bends, we estimate a loss of about 0.4 and 0.6 km of fault slip. Considering these decreases in slip we estimate across the anticlinal fault bends, a dip-slip rate for the higher levels of

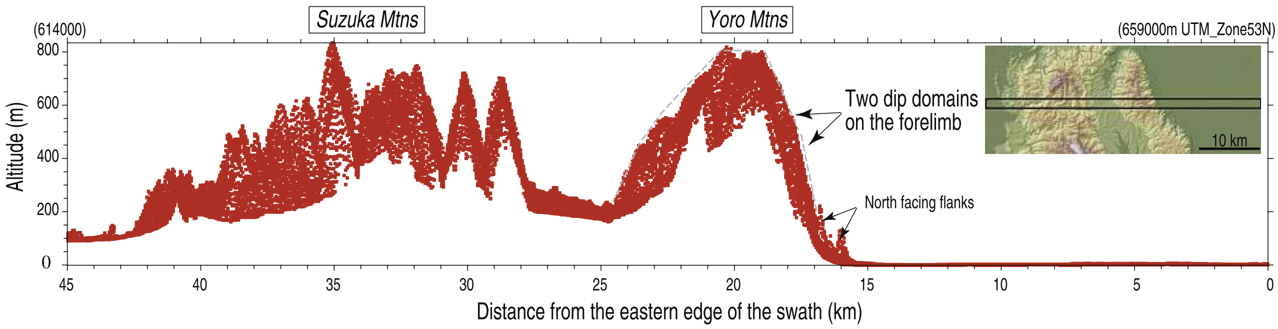

Figure 16. Topography of the Yoro and Suzuka Mountains based on 50-m DEM contained within a 1.5 km × 40 km swath. Topography of the Yoro Mountains suggests a smoothed stripped unconformity below the Pliocene-Pleistocene sedimentary cover. The eastern flank of the Yoro Mountains that forms the forelimb of the basement-involved fold is further subdivided into two dip domains, whereas topography of the western flank of the mountains indicates an upward concave shape of the backlimb.

the structure is calculated to be 3.2 ± 0.1 mm/yr, with an average vertical rate of 1.2 ± 0.1 mm/yr.

[39] The kinematic solution for the Yoro basement-involved wedge thrust structure and age controls from folded Holocene units allow slip rates to be determined for the blind thrust at shorter timescales. Correlation between boreholes [*Nakanishi*, 2003] and reflectors in the S wave seismic profile across the fold scarp yields 30 m of apparent structural relief for the 15.5 ± 1.2 ka alluvial fan deposits uplifted by slip on the lower ramp. Assuming that the 0.023 degree gradient of the modern alluvial fan (Figure 6) is a reasonable proxy for the paleostream gradient, the original topographic relief between the lowest and highest points of this horizon along a distance of ~250 m is estimated to be 5.6 m. Subtraction of this assumed topographic relief prior to folding from the apparent structural relief yields a value of 24.4 m of vertical apparent offset on this horizon. Taking a true dip of 27° For the shallower portion of the oblique ramp, we determine a dip-slip rate of 3.5 ± 0.3 mm/yr r at intermediate (10^4 years) timescales, with an average vertical rate of 1.5 ± 0.2 mm/yr. This is consistent with shorter-term (10^3 years) slip rates calculated by a structural relief across a circa 7.2–7.3 ka volcanic ash (K-Ah [*Machida and Arai*, 2003]) horizon (1.5 ± 0.1 mm/yr) contained in boreholes A and B [*Nakanishi*, 2003].

[40] The dip-slip rate at intermediate (10^4 years) timescales and short (10^3 years) timescales estimated at the highest level of the structure is also consistent with those at millennial timescales, indicating that this basement-involved wedge thrust structure has accommodated strains at a constant rate since the onset of structural growth.

6.2. Coseismic Folding Generated by Historic Blind Thrust Earthquake on the Yoro Thrust

[41] The structural solution for the Yoro basement-involved fold suggests that the coseismic fold scarp with a height of about 2 m is located coincident with the upward projection of the active synclinal axial surface formed above the east vergent wedge tip (Figure 15). The borehole transect across the fold scarp shows that at least three uplift events are recorded by Holocene sediment beneath the fold scarp and that the topographic scarp there formed during the latest historic event in A.D. 1586.

[42] We attribute the uplift events recorded in the folded historic and late Holocene units as evidence for growth of the coseismic fold scarp in past earthquakes above the basement-involved wedge thrust fold (Figure 17). Key observations include (1) sedimentary units that thicken across the scarp and (2) structural relief on a topographic fold scarp that is coincident with the active synclinal axial surface (above the wedge tip) defined by older strata. In addition, the width of strata folded in the forelimb narrows upward in a growth triangle [*Suppe et al.*, 1992]. The width of the east dipping forelimb as measured in the youngest folded deposit (unit 1; floodplain sand and mud) is less than 20 m wide at the ground surface, whereas it is 40 m wide across unit 2 (peat deposits) at 5 m depth, and 100 m wide as measured on late Pleistocene alluvial fan deposits at 40 m depth. This observation indicates bed-by-bed growth of coseismic fold scarps above the basement-involved wedge thrust albeit by numerous earthquakes between dated stratigraphic intervals.

[43] Another key observation is that strata folded at the base of the forelimb curve gently upward across a broad zone of folding, suggesting that it is not a classic fault bend fold with sharp hinges. Moreover, the 20 m wide forelimb defined at the ground surface, which we have shown to be produced by a single event in A.D. 1586, is an unrealistic amount of fault slip for an earthquake of this magnitude. Given a wedge thrust fold solution for the structure, we interpret the apparently large width of the forelimb at the ground surface as evidence for growth by kink band migration across a curved synclinal hinge [*Suppe et al.*, 1997], rather than by progressive limb rotation [*Riba*, 1976].

[44] While the easternmost pair of entry and exit active synclinal axial surfaces extending from the tip of the basement thrust wedge is ‘‘fixed’’ at the base of the coseismic fold scarp, corresponding inactive axial surfaces move up onto the forelimb as coseismic slip is accrued during repeated blind thrust earthquakes. This model predicts a more gentle dipping and narrower forelimb in the youngest historic horizon produced by the latest earthquake and steeper and wider forelimbs of older and deeper horizons that have been folded during multiple earthquakes in the past (Figure 17).

[45] This kinematic interpretation of the fold scarp provides insight into bed-by-bed growth of the fold limbs recorded by a fold scarp geomorphology. The fold scarp formed by the growth of the fold limb during the penultimate paleoseismic event has been partly removed by erosion due to a change in base level associated with a fall in regional sea level, as suggested by a sinuous east facing terrace riser between the lower and higher Holocene terraces, and a buttress unconformity between unit 1 and 2. Subsequent deposition of unit 1 buttressing against the terrace riser was followed by coseismic folding during the latest paleoseismic event, which formed the frontal scarp that separates the lower Holocene terrace from modern alluvial plain. This kinematic interpretation of structural growth of the coseismic fold scarp and subsurface stratigraphy thus indicate that the fold scarp has formed as a convolution of bed-by-bed coseismic growth of fold limbs and deposition, and/or erosion events between discrete earthquake events.

[46] Perhaps most interestingly, similar coseismic fold scarps are found at the base of the forelimbs of adjacent active folds in the NIFZ such as Kuwana anticline and Yokkaichi anticline (Figure 3). Analysis of folded strata defined by borehole transects and radiocarbon dating suggest that most, if not all, of these scarps, formed during the historic A.D. 1586 earthquake [*Sugai et al.*, 1998, 1999a; *Togo*, 2000; *Ishiyama et al.*, 2002b]. Kuwana anticline, located south of the Yoro structure, has also formed as an east vergent basement-involved wedge thrust fold. This indicates that, in spite of en echelon pattern of these active folds, they did not rupture independently but transferred slip from one ramp to the next (i.e., multisegment rupture) during the historic earthquake in A.D. 1586. The NIFZ thus demonstrates the potential for more hazardous, multi-segment ruptures rather than single segment earthquakes such as 1982–1985 California earthquake sequence (the 1981 New Idria (Mw 5.4), 1983 Coalinga (Mw 6.5), and

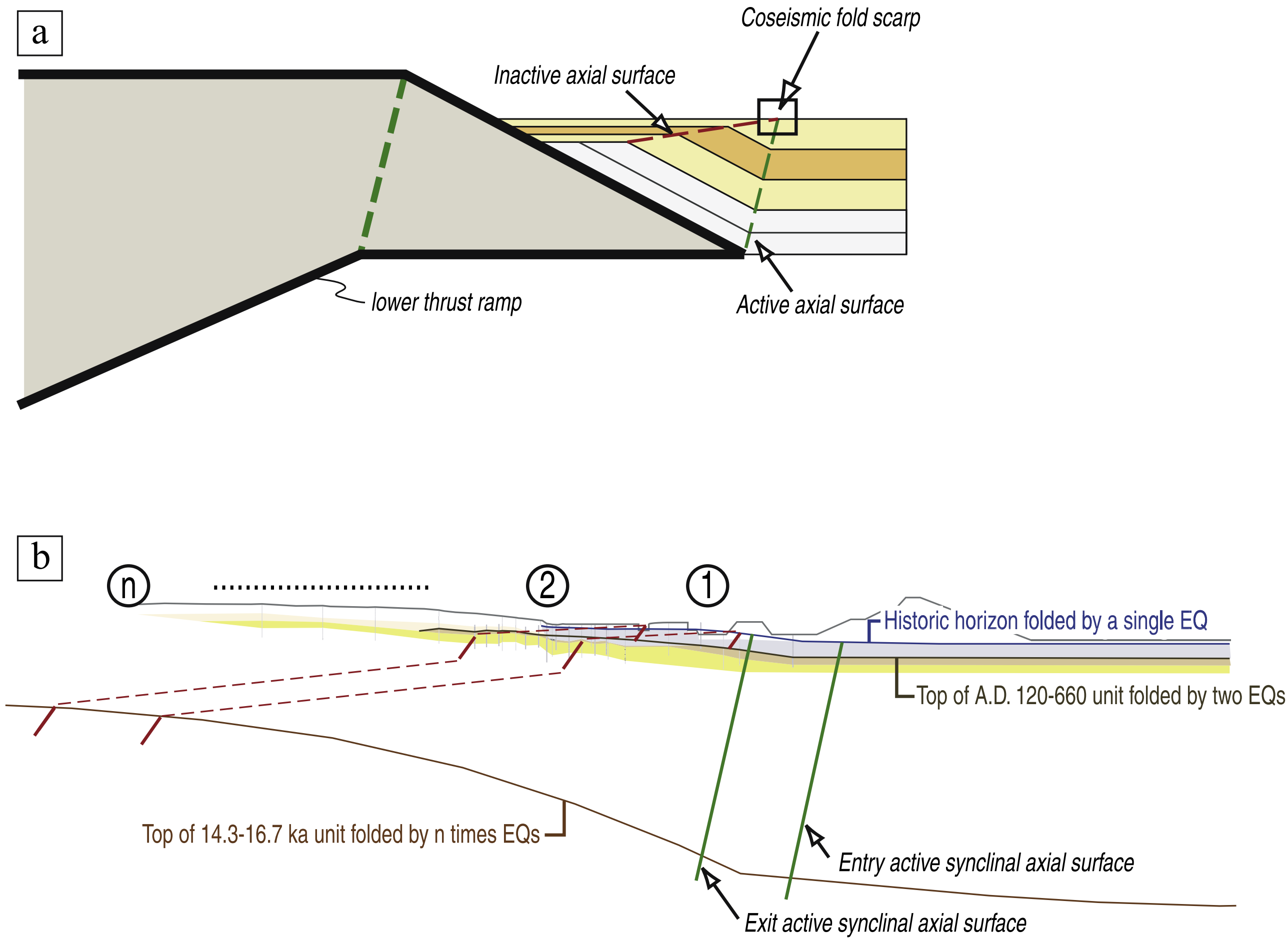

Figure 17. (a) Schematic cross section that explains the fold scarp topography above a basement-involved wedge thrust fold. (b) Application of kink band migration across curved hinges to the cross section of the coseismic fold scarp at Shizu site. No vertical exaggeration. Coseismic slip by repeated large earthquakes on the east vergent wedge thrust explains a bed-by-bed growth of the fold scarp, comprised by a more gently dipping and narrower forelimb in the youngest historic horizon produced by the latest earthquake and steeper and wider forelimbs of older and deeper horizons that has been folded during multiple earthquakes in the past. Exit and entry inactive axial surfaces associated with the latest, recent two, and n times earthquakes are denoted by numbers within circles.

1985 Kettleman Hills (Mw 6.1) earthquakes) [*Stein and Ekstrom*, 1992].

7. Conclusions

[47] Our study shows that integration of multiscale structural analyses based on high-resolution seismic reflection data, tectonic geomorphology and geochronology can define the detailed kinematic evolution, subsurface geometry and coseismic growth of active fold scarps and their link with underling blind thrusts. The close coincidence between the coseismic fold scarp generated by historic earthquakes above the Yoro basement-involved fold and the underlying thrust geometry provides confidence in assigning coseismic deformation mechanisms that have acted to build the structure. For the Yoro structure we conclude that it has grown above a thick-skinned wedge thrust that is consistent with geologic mapping on the backlimb, and borehole stratigraphy in the Nobi Basin, and folded fluvial terraces on the backlimb. On the basis of structural relief of strata of known ages, the slip rate of the Yoro thrust at long-term (10^6 years) and intermediate (10^4 years) timescales are calculated to be about 3.2 ± 0.1 mm/yr and 3.5 ± 0.3 mm/yr, suggesting that this structure has accommodated strain at an essentially constant rate since the onset of structural growth. In addition, coseismic fold scarps of the A.D. 1586 earthquake coincide with the projected surface trace of the east vergent wedge thrust tip at the leading edge of the Yoro basement-involved fold. Fold scarps generated by the most recent and penultimate earthquakes can be restored in a bed-by-bed fashion, based on curved hinge kink band migration at the actively propagating wedge tip. This suggests that coseismic fold scarps at the ground surface may be indicators of slip on underlying blind thrust faults, and may be used to characterize these otherwise inaccessible seismic hazards. In addition, most, if not all, of the coseismic fold scarps formed during the historic A.D. 1586 earthquake can be traced along the en echelon thrust system, which emphasizes the potential risk of multisegment ruptures in similar active thrust belts.

[48] **Acknowledgments.** We thank Toshimichi Nakanishi, Atsumasa Okada, Shigeru Toda, Hajime Kato, Tomoo Echigo, Shinsuke Okada, Nobuhisa Matsuta, Hiroyuki Tsutsumi, Nobuhiko Sugito, Nobumasa Suzuki, Haruo Kimura, and colleagues at Aichi Educational University, University of Tokyo, and Kyoto University for invaluable assistance with acquisition of seismic data and discussion. Daisaku Kawabata is also thanked for providing us with a high-resolution shaded relief map. Finally, our thanks go to Associate Editor James F. Dolan, Tom Pratt, and an anonymous reviewer for their constructive reviews, which greatly improved the manuscript. Seismic data acquisitions B-B' and C-C' were funded by JSPS Grants-in-Aid for Scientific Research 16200050 to A. Okada and Ishiyama, and C-C' was done as a part of Special Project for Earthquake Disaster Mitigation in Urban Areas funded by Ministry of Education, Culture, Sports, Science and Technology.

References

Allmendinger, R. W. (1998), Inverse and forward numerical modeling of trishear fault-propagation folds, *Tectonics*, *17*, 640–656.

Apotria, T. G., W. T. Suedden, J. H. Spang, and D. V. Wiltschko (1992), Kinematic models of deformation at an oblique ramp, in *Thrust Tectonics*, edited by K. R. McClay, pp. 141–151, CRC Press, Boca Raton, Fla.

Atwater, B. F., et al. (2001), Grouted sediment slices show signs of earthquake shaking, *Eos Trans AGU*, *82*(49), 603.

Awata, Y., and F. Yoshida (1991), Holocene movement of the Kuwana and Yokkaichi faults, northwest of Ise Bay, central Japan (in Japanese), *Active Fault Res.*, *9*, 61–68.

Benedetti, L., P. Tapponnier, G. C. P. King, B. Meyer, and I. Manighetti (2000), Growth folding and active thrusting in the Montello region, Veneto, northern Italy, *J. Geophys. Res.*, *105*, 739–766.

Benedetti, L. C., P. Tapponnier, Y. Gaudemer, I. Manighetti, and J. Van der Woerd (2003), Geomorphic evidence for an emergent active thrust along the edge of the Po Plain: The Broni-Stradella fault, *J. Geophys. Res.*, *108*(B5), 2238, doi:10.1029/2001JB001546.

Bennett, E. R., J. H. Youngson, J. A. Jackson, R. J. Norris, G. M. Raisbeck, F. Yiou, and E. Fielding (2005), Growth of South Rough Ridge, Central Otago, New Zealand: Using in situ cosmogenic isotopes and geomorphology to study an active, blind reverse fault, *J. Geophys. Res.*, *110*, B02404, doi:10.1029/2004JB003184.

Bullard, T. F., and W. R. Lettis (1993), Quaternary fold deformation associated with blind thrust faulting, Los Angeles basin, California, *J. Geophys. Res.*, *98*, 8349–8369.

Burbank, D., A. Meigs, and N. Brozović (1996), Interactions of growing folds and coeval depositional systems, *Basin Res.*, *8*, 199–223.

Champion, J. A., A. Tate, K. J. Mueller, and M. Guccione (2001), Geometry, numerical modeling and revised slip rate for the Reelfoot blind thrust and trishear fault-propagation fold, New Madrid seismic zone, *Eng. Geol.*, *62*, 31–49.

Committee for Subsurface Structure of the Nobi Basin (2001), Report on survey for subsurface structure of the Nobi basin (in Japanese), report, 13 pp., Nagoya, Japan.

Dolan, J. F., S. A. Christofferson, and J. H. Shaw (2003), Recognition of paleoearthquakes on the Puente Hills blind thrust fault, California, *Science*, *300*, 115–118.

Dominguez, S., J. Avouac, and R. Michel (2003), Horizontal coseismic deformation of the 1999 Chi-Chi earthquake measured from SPOT satellite images: Implications for the seismic cycle along the western foothills of central Taiwan, *J. Geophys. Res.*, *108*(B2), 2083, doi:10.1029/2001JB000951.

Erslev, E. A. (1991), Trishear fault-propagation folding, *Geology*, *19*, 617–620.

Freymueller, J., N. E. King, and P. Segall (1994), The co-seismic slip distribution of the Landers earthquake, *Bull. Seismol. Soc. Am.*, *84*, 646–659.

Furusawa, A. (1990), Volcanic ash layers of the Tokai Group and the Ama and Yatomi Formations under the Nobi Plain, and their correlation (in Japanese with English abstract), *J. Geol. Soc. Jpn.*, *96*, 883–901.

Glen, J. M., and R. S. Coe (1997), Paleomagnetism and magnetic susceptibility of Pleistocene sediments from drill hole OL-92, Owens Lake, CA, in *An 800,000–Year Paleoclimatic Record from Core OL-92, Owens Lake, Southeast California*, edited by G. I. Smith and J. L. Bischoff, *Spec. Pap. Geol. Soc. Am.*, *317*, 67–78.

Groshong, R. H. (2006), *3-D Structural Geology*, 400 pp., Springer, New York.

Harayama, S., M. Miyamura, F. Yoshida, K. Mimura, and F. Kurimoto (1989), Geology of the Gozaishoyama district, with geologic sheet map at 1:50,000 (in Japanese with English abstract), report, 145 pp., Geol. Surv. of Jpn., Tsukuba.

Hardy, S., and M. Ford (1997), Numerical modeling of trishear fault-propagation folding, *Tectonics*, *16*, 841–854.

Hung, J., and J. Suppe (2002), Subsurface geometry of the Sani-Chelungpu faults and fold scarp formation in the 1999 Chi-Chi Taiwan earthquake, *Eos Trans AGU*, *83*(47), Fall Meet. Suppl., Abstract T61B-1268.

Ikeda, Y., T. Imaizumi, H. Sato, M. Togo, K. Hirakawa, and T. Miyauchi (Eds.) (2002), *Atlas of Quaternary Thrust Faults in Japan* (in Japanese), 254 pp., Univ. Tokyo Press, Tokyo.

Ishiyama, T., K. Takemura, and A. Okada (1999), Structural growth rate of the western margin of the Suzuka Range during Quaternary (in Japanese with English abstract), *J. Seismol. Soc. Jpn.*, *52*, 229–240.

Ishiyama, T., K. J. Mueller, M. Togo, K. Takemura, and A. Okada (2002a), Geomorphology and kinematics of the Nobi-Ise active fault zone, central Japan: Implications for the kinematic growth of tectonic landforms within an active thrust belt, *Eos Trans. AGU*, *83*(47), Fall Meet. Suppl., Abstract S11B-1140.

Ishiyama, T., M. Togo, T. Imaizumi, H. Sato, T. Nakata, T. Nohara, and T. Haraguchi (2002b), Evolution of fault-related landform associated with late Holocene faulting on the Yoro fault, revealed by drilling survey at Shizu-Shobuhara Site, Nan-no Town, Gifu Prefecture, central Japan (in Japanese with English abstract), *Active Fault Res.*, *22*, 115–126.

Ishiyama, T., K. Mueller, M. Togo, A. Okada, and K. Takemura (2004), Geomorphology, kinematic history, and earthquake behavior of the active Kuwana wedge thrust anticline, central Japan, *J. Geophys. Res.*, *109*, B12408, doi:10.1029/2003JB002547.

Johnson, K. M., Y. J. Hsu, P. Segall, and S. B. Yu (2001), Fault geometry and slip distribution of the 1999 Chi-Chi, Taiwan earthquake imaged from inversion of GPS data, *Geophys. Res. Lett.*, *28*, 2285–2288.

Kawabata, D., and T. Ishiyama (2006), Digital photogrametry of late Holocene fold scarps along the Yoro fault, paper presented at Japan Geoscience Union Meeting, Chiba.

Kelson, K. I., G. D. Simpson, R. B. VanArsdale, C. C. Haraden, and W. R. Lettis (1996), Multiple late Holocene earthquakes along the Reelfoot fault, central New Madrid seismic zone, *J. Geophys. Res.*, *101*, 6151–6170.

Kishimoto, K. (2000), Combined bathymetric and topographic mesh data: Japan 250 m. grid, *Open File Rep. 353*, 1-CD-ROM, Geol. Surv. of Jpn., Tsukuba.

Lavé, J., and J. P. Avouac (2000), Active folding of fluvial terraces across the Siwaliks Hills, Himalayas of central Nepal, *J. Geophys. Res.*, *105*, 5735–5770.

Lee, J. C., C. Rubin, K. Mueller, Y. G. Chen, Y. C. Chan, K. Sieh, H. T. Chu, and W. S. Chen (2004), Quantitative analysis of movement along an earthquake thrust scarp: A case study of a vertical exposure of the 1999 surface rupture of the Chelungpu fault at Wufeng, western Taiwan, *J. Asian Earth Sci.*, *23*, 263–273.

Machida, H., and F. Arai (2003), *Atlas of Tephra in and Around Japan* (in Japanese), 336 pp., Univ. of Tokyo Press, Tokyo.

Medwedeff, D. A. (1992), Geometry and kinematics of an active, laterally propagating wedge thrust, Wheeler Ridge, California, in *Structural Geology of Fold and Thrust Belts*, edited by S. Mitra and G. W. Fisher, pp. 3–28, Johns Hopkins Univ. Press, Baltimore, Md.

Medwedeff, D. A., and J. Suppe (1997), Multibend fault-bend folding, *J. Struct. Geol.*, *19*, 279–292.

Miyamura, M., K. Mimura, and T. Yokoyama (1976), Geology of the Hikone-Tobu district, with geologic sheet map at 1:50,000 (in Japanese with English abstract), 49 pp., Geol. Surv. of Jpn., Tsukuba.

Molnar, P., et al. (1994), Quaternary climatic change and the formation of river terraces across growing anticline on the north flank of the Tien Shan, *J. Geol.*, *102*, 583–602.

Mueller, K., and J. Suppe (1997), Growth of Wheeler Ridge anticline, California: Geomorphic evidence for fault-bend-folding behavior during earthquakes, *J. Struct. Geol.*, *19*, 383–396.

Mueller, K., J. Champion, M. Guccione, and K. Kelson (1999), Fault slip rates in the modern New Madrid seismic zone, *Science*, *286*, 1135–1138.

Nakanishi, T. (2003), Detection of multiple paleoseismic events based on high-resolution sedimentological core analysis, thesis for Doctor of Science, 131 pp., Kyoto Univ., Kyoto, Japan, March.

Nakata, T., and T. Imaizumi (Eds.) (2002), Digital active fault map of Japan (in Japanese), 60 pp., Univ. of Tokyo Press, Tokyo.

Nakata, T., and K. Shimazaki (1997), Geo-slicer as a tool for active fault research (in Japanese with English abstract), *J. Geogr.*, *106*, 59–69.

Okada, A., and M. Togo (Eds.) (2000), *Active Faults in the Kinki Area, Central Japan: Sheet Maps and Inventories*, 395 pp., Univ. of Tokyo Press, Tokyo.

Philip, H., and M. Meghraoui (1983), Structural analysis and interpretation of the surface deformations of the El Asnam earthquake of October 10, 1980, *Tectonics*, *2*, 17–49.

Philip, H., E. Rogozhin, A. Cisternas, J. C. Bousquet, B. Borisov, and A. Karakhanian (1992), The Armenian earthquake of 1988 December 7: Faulting and folding, neotectonics and paleoseismicity, *Geophys. J. Int.*, *110*, 141–158.

Pratt, T. L., J. H. Shaw, J. F. Dolan, S. A. Christofferson, R. A. Williams, J. K. Odum, and A. Plesch (2002), Shallow seismic imaging of folds above the Puente Hills blind-thrust fault, Los Angeles, California, *Geophys. Res. Lett.*, *29*(9), 1304, doi:10.1029/2001GL014313.

Research Group for Active Faults (1991), *Active Faults in Japan: Sheet Maps and Inventories* (in Japanese), 437 pp., Univ. of Tokyo Press, Tokyo.

Riba, O. (1976), Syntectonic unconformities of Alto Cardener, Spanish Pyrenees–genetic interpretation, *Sediment. Geol.*, *15*, 213–233.

Rockwell, T. K., E. A. Keller, M. N. Clark, and D. L. Johnson (1984), Chronology and rates of faulting of Ventura River terraces, California, *Geol. Soc. Am. Bull.*, *95*, 1466–1474.

Rockwell, T. K., E. A. Keller, and G. R. Dembroff (1988), Quaternary rate of folding of the Ventura Avenue anticline, western Transverse Ranges, southern California, *Geol. Soc. Am. Bull.*, *100*, 850–858.

Sakamoto, T., Y. Takada, T. Kuwabara, and J. Itoigawa (1986), Geology of the Nagoya-Nambu district, with geologic sheet map at 1:50,000 (in Japanese with English abstract), 55 pp., Geol. Surv. of Jpn., Tsukuba.

Sato, H., et al. (1997), Evolution of the active Senya thrust fault, northern Honshu, Japan. Abstracts 1997, 185, Seismol. Soc. of Jpn., Tokyo.

Scharer, K. M., D. Burbank, J. Chen, and R. Weldon (2006), Kinematic models of fluvial terraces over active detachment folds: Constraints on the growth mechanism of the Kashi-Atushi fold system, Chinese Tian Shan, *Geol. Soc. Am. Bull.*, *118*, 1006–1021.

Shaw, J., and J. Suppe (1994), Active faulting and growth folding in the eastern Santa Barbara Channel, California, *Geol. Soc. Am. Bull.*, *106*, 607–626.

Shaw, J. H., and J. Suppe (1996), Earthquake hazards of active blind-thrust faults under the central Los Angeles basin, California, *J. Geophys. Res.*, *101*, 8623–8642.

Shaw, J. H., A. Plesch, J. F. Dolan, T. L. Pratt, and P. Fiore (2002), Puente Hills blind-thrust system, Los Angeles, California, *Bull. Seismol. Soc. Am.*, *92*, 2946–2960.

Shaw, J. H., C. Connors, and J. Suppe (Eds.) (2005), Seismic interpretation of contractional fault-related folds, *AAPG Stud. Geol.*, *53*, 157 pp.

Shyu, J. B. H., K. Sieh, J.-P. Avouac, W.-S. Chen, and Y.-G. Chen (2006), Millennial slip rate of the Longitudinal Valley fault from river terraces: Implications for convergence across the active suture of eastern Taiwan, *J. Geophys. Res.*, *111*, B08403, doi:10.1029/2005JB003971.

Stein, R. S., and G. Ekstrom (1992), Seismicity and geometry of a 110-km-long blind thrust fault: 2. Synthesis of the 1982–1985 California earthquake sequence, *J. Geophys. Res.*, *97*, 4865–4883.

Stuiver, M., and P. J. Reimer (1993), Extended 14C database and revised CALIB radiocarbon calibration program, *Radiocarbon*, *35*, 215–230.

Sugai, T., Y. Awata, and K. Shimokawa (1998), Paleoseismological study of the Kuwana fault and the Yokkaichi fault in Mie Prefecture, central Japan (in Japanese with English abstract), *Interim Rep. EQ/98/1*, pp. 75–90, Geol. Surv. of Jpn., Tsukuba.

Sugai, T., Y. Fusejima, Y. Awata, T. Azuma, Y. Kariya, and Y. Suzuki (1999a), Late Holocene paleoseismicity of the Yoro fault system, central Japan (in Japanese with English abstract), *Interim Rep. EQ/99/3*, pp. 89–102, Geol. Surv. of Jpn., Tsukuba.

Sugai, T., Y. Sugiyama, and K. Mizuno (1999b), 900,000–year cyclostratigraphic record from a 600 m core, GS-NB-1, the Nobi basin, central Japan (in Japanese with English abstract), *Interim Rep. EQ/99/3*, pp. 69–76, Geol. Surv. of Jpn., Tsukuba.

Suppe, J. (1983), Geometry and kinematics of fault-bend folding, *Am. J. Sci.*, *283*, 684–721.

Suppe, J., and D. Medwedeff (1990), Geometry and kinematics of fault-propagation folding, *Ecologae Geol. Helv.*, *83*, 409–454.

Suppe, J., G. T. Chou, and S. C. Hook (1992), Rates of folding and faulting determined from growth strata, in *Thrust Tectonics*, edited by K. R. McClay, pp. 105–121, CRC Press, Boca Raton, Fla.

Suppe, J., F. Sàbat, J. A. Muñoz, J. Poblet, E. Roca, and J. Vergés (1997), Bed-by-bed fold growth by kink-band migration: Sant Llorenç de Morunys, eastern Pyrenees, *J. Struct. Geol.*, *19*, 443–461.

Suppe, J., Y. H. Lee, Y. G. Chen, and J. H. Hung (2000), Coseismic fault-bend folding: Fold scarp formation in the 1999 Chi-Chi earthquake (M 7.6), Taiwan fold-and-thrust belt, *Eos Trans. AGU*, *81*(48), 874.

Takada, Y., Y. Kondo, and M. Miyamura (1979), Geology of the Tsushima district, with geologic sheet map at 1:50,000 (in Japanese with English abstract), 56 pp., Geol. Surv. of Jpn., Tsukuba.

Takemura, K. (1985), The Plio-Pleistocene Tokai Group and the tectonic development around Ise Bay of central Japan since Pliocene, *Mem. Fac. Sci. Kyoto Univ. Ser. Geol. Mineral.*, *51*, 21–96.

Thompson, S. C., R. J. Weldon, C. M. Rubin, K. Abdrakhmatov, P. Molnar, and G. W. Berger (2002), Late Quaternary slip rates across the central Tien Shan, Kyrgyzstan, central Asia, *J. Geophys. Res.*, *107*(B9), 2203, doi:10.1029/2001JB000596.

Togo, M. (2000), *Geomorphological Analysis on Surface Ruptures by Reverse Faulting in Japan* (Bisyo-chikei-niyoru-katsudansou-handoku) (in Japanese), 206 pp., Kokon, Tokyo.

Umitsu, M. (1994), *Late Quaternary Environment and Landform Evolution of Riverine Coastal Lowlands* (in Japanese), 270 pp., Kokon, Tokyo.

Usami, T. (2003), *Materials for Comprehensive List of Destructive Earthquakes in Japan, 416–2001* (in Japanese), 603 pp., Univ. of Tokyo Press, Tokyo.

Wei, D., and T. Seno (1998), Determination of the Amurian plate motion, in *Mantle Dynamics and Plate Interactions in East Asia*, *Geodyn. Ser.*, vol. 27, edited by M. F. J. Flower et al., pp. 337–346, AGU, Washington, D. C.

Yeats, R. S., K. Sieh, and C. R. Allen (1997), *The Geology of Earthquakes*, 568 pp., Oxford Univ. Press, New York.

Yilmaz, O. (1987), *Seismic Data Processing*, 526 pp., Soc. of Explor. Geophys., Tulsa, Okla.

Yoshida, F. (1984), Geology of the Yokkaichi district, with geologic sheet map at 1:50,000 (in Japanese with English abstract), 81 pp., Geol. Surv. of Jpn., Tsukuba.

Yoshida, F. (1988), Plio-Pleistocene Tokai Group between the Suzuka and Yoro Mountains, central Japan (in Japanese with English abstract), *J. Earth Sci.*, *42*, 1–16.

Yoshida, F., C. Kurimoto, and M. Miyamura (1991), Geology of the Kuwana district, with geologic sheet map at 1:50,000 (in Japanese with English abstract), 154 pp., Geol. Surv. of Jpn., Tsukuba.

T. Ishiyama, Active Fault Research Center, Geological Survey of Japan, National Institute of Advanced Industrial Science and Technology, Site 7, 1-1-1 Higashi, Tsukuba, Ibaraki 305-8567, Japan. (t-ishiyama@aist.go.jp)

K. Mueller, Department of Geological Sciences, University of Colorado, Boulder, CO 80309-0399, USA. (karl.mueller@colorado.edu)

H. Sato, Earthquake Research Institute, University of Tokyo, 1-1-1, Yayoi, Bunkyo-ku, Tokyo 113-0032, Japan. (satow@eri.u-tokyo.ac.jp)

M. Togo, Department of Geoscience, Hosei University, Aihara-Cho, 4342, Machida 194-0298, Japan. (togo_m@mt.tama.hosei.ac.jp)